CHAPTER ONE

Past, present, and future of joint utilization of experimental, empirical, and computed spectroscopic data: Challenges, advantages, and recommendations

Roland Tóbiás[a,b,*], **Tibor Furtenbacher**[a,*], **and Attila G. Császár**[a,b,*]
[a]Institute of Chemistry, ELTE Eötvös Loránd University, Budapest, Hungary
[b]HUN-REN–ELTE Complex Chemical Systems Research Group, Budapest, Hungary
*Corresponding authors. e-mail address: roland.tobias@ttk.elte.hu; furtibu@staff.elte.hu; attila.csaszar@ttk.elte.hu

Contents

Abstract

As evidenced by the massive number of their users, line-by-line spectroscopic databases are indispensable for scientists and engineers working in many fields. To ensure the high accuracy of line-by-line data, both advanced experimental (ultra)high-resolution spectroscopy techniques and sophisticated empirical/theoretical approaches are required. This study provides a review about the combined use of experimental,

Advances in Quantum Chemistry, Volume 94
ISSN 0065-3276, https://doi.org/10.1016/bs.aiq.2025.01.002
Copyright © 2026 Elsevier Inc. All rights are reserved, including those for text and data mining, AI training, and similar technologies.

empirical, and theoretical spectroscopic data, emphasizing the considerable advantages resulting from a joint treatment. In particular, employing the (C)W2024 database of $H_2{}^{16}O$ transitions and empirical energy levels, significant problems with experimental data, such as typographical errors, miscalibrations, underestimated uncertainties, and misinterpretation of observed peaks, are discussed. Issues with (semi-) empirical data, determined *via* Ritz-based and effective-Hamiltonian procedures, are outlined next. Following a brief description about the current state of first-principles computations, a few examples are given where complex spectral features are misinterpreted. In all cases, feasible solutions to the problems identified are presented. Finally, to avoid similar issues in future publications, recommendations are made for providers of high-resolution spectroscopic data, as well as for computational spectroscopists and database providers.

1. Introduction

Besides computers, few tools have been invented by mankind which proved to be as valuable for science and technology as spectrometers. During the last two centuries, scientific and technological developments were hugely impacted by these ever-evolving instruments.[1] In simple terms, spectroscopy is the science of studying the interaction of matter with electromagnetic radiation, from the shortest to the longest wavelengths (in all phases, though here we are concentrating on the gas phase). Several reasons can be given why detailed high-resolution rovibronic spectroscopic information, the topic of this article, is so important for humanity.[2–4] For example, spectroscopy is indispensable to understand various natural and artificial environments surrounding us, be it on Earth or in our (expanding) universe. Atmospheric research (radiative transfer), astrophysics and astrochemistry (star formation, (exo)planetary atmospheres, interstellar medium), medical (breath analysis), communication, remote-sensing, and space-mission science and engineering all use spectroscopic data extensively. Modeling of all these vastly different environments is also based, at least partially, on the availability of detailed, often line-by-line spectroscopic data.

To equip the very large community of users of reliable rovibronic spectroscopic information, during the last half of a century it became common to deposit spectroscopic data in validated, annotated, and regularly updated spectroscopic databases, such as (in alphabetical order) AFCRL,[5] CDMS (Cologne Database for Molecular Spectroscopy),[6] ExoMol,[7,8] GEISA,[9] HITRAN (high-resolution transmission molecular absorption),[4,10] which the Budapest group has been contributing to for

about a decade,[4,11,12] and JPL.[13] Note that the authors of this article maintain their own spectroscopic information system. It is part of ReSpecTh, a catalog containing reaction kinetics (Re), high- resolution spectroscopy (Spec), and thermochemical (Th) data, with tools facilitating the use of its information content (see https://respecth.elte.hu).

Assembling large line-by-line spectroscopic databases always involves the treatment of data of heterogeneous (experimental, empirical, and computational) origin. These data are characterized, among other important differences, by vastly different accuracies. The uncertainty range of these heterogeneous data extends from a few tenths of kHz (for the most accurately measured Lamb-dip frequencies)[14,15] to 1–2 cm^{-1} (for the best first-principles computation of rovibronic wavenumbers),[2] that is 8–9 orders of magnitude. This extent of heterogeneity naturally gives rise to a number of issues during the comprehensive, joint analysis of all these data. Needless to say, as the sophistication of the experimental, empirical, and theoretical approaches changed, the interplay between these data sources also changed significantly. Measuring molecular spectra at high resolution and the interpretation of spectral features developed substantially during the last decades.[1] Nevertheless, the information provided by these measurements remained basically the same: line positions, line assignments, line intensities, line widths, as well as self- and foreign shifts caused by the environment of the absorbing or emitting molecule. All this information is stored in the most widely used line-by-line spectroscopic databases,[4–10] HITRAN[4] being the canonical one. These extensive datasets are scrutinized carefully by new experiments and get updated on a regular basis; for example, every four years in the case of HITRAN.

Compact representation of measured line positions and intensities has traditionally been achieved *via* effective Hamiltonians (EH).[16] The EHs of various form contain a relatively small number of adjustable parameters, refined based on the available experimental information; thus, these spectroscopic parameters change regularly when new experimental information becomes available. The EH approach works extremely well for heavier species and for lower rovibrational excitations and it is an excellent source of (semi-)empirical spectroscopic results. Based upon its design, the EH approach works much better when it interpolates than when it extrapolates. Occasionally, it may have significant accuracy issues, as shown for the case of the NH_3 molecule,[17] discussed briefly below.

An alternative representation of the experimental line positions is provided by the upper and lower states of observed transitions, relying only on

the Ritz principle.[18] Employing an inversion scheme for the transition frequencies, the underlying energy levels can be determined with practically the same accuracy characterizing the experimental results. One such inversion protocol, developed in our group, is called MARVEL, where the abbreviation stands for Measured Active Rotational-Vibrational Energy Levels.[19–22,23] The MARVEL procedure results in empirical energy values accompanied by individual uncertainties and confidence intervals.[23] During the last decade, our group performed MARVEL analyses for a large number of spectra measured for numerous molecules, including diatomics ($^{12}C_2$,[24,25] ^{12}CH,[26] ^{14}NH,[27] ^{16}OH,[26] $^{16}O_2$,[28] $^{48}Ti^{16}O$,[29] and $^{90}Zr^{16}O$[30]), triatomics (several CO_2 isotopologues,[31,32] three H_3^+ isotopologues,[33,34] nine water isotopologues,[23,35–42] two $H^{16}OCl$ isotopologues,[43,44] $H_2{}^{16}S$,[45] $^{14}N_2{}^{16}O$,[46] as well as four $S^{16}O_2$ isotopologues),[47] tetratomics ($^{12}C_2H_2$,[48] $H_2{}^{12}C^{16}O$,[49] and $^{14}NH_3$[50]), and even a pentatomic molecule, $H_2{}^{12}C_2{}^{16}O$.[51] The MARVEL approach has been described at several stages of its development and has been reviewed several times, as well.[22,23,52–54]

The formulation of the MARVEL scheme heavily utilizes the theory of spectroscopic networks (SN).[52,54,55] SNs are weighted, directed, loop-free multigraphs, where (a) the nodes are energy levels, (b) the edges are rovibronic transitions, directed from their lower energy levels to their upper ones, and (c) nonnegative edge weights are attached to the transitions (more generally, node and edge weights are selected for the actual task the SN approach is applied for). The most important elements of an SN are (a) components (sets of energy levels not linked by transitions), (b) paths (sequences of connected, unrepeated lines and states), (c) cycles (series of connected transitions and energy levels, where every rovibronic state has two neighboring energy levels), and (d) bridges (lines whose deletion increases the number of components). The energy levels of the various components are not connected by definition. Within a component, the relative energy values of the states are defined with respect to the lowest-energy level in that component. When this is the lowest-energy level of a nuclear-spin isomer of the given molecule, this component is a principal component, otherwise it is a floating component.

As to the accuracy of first-principles variational nuclear-motion computations, as of today, that is in the fourth age of quantum chemistry,[56] we distinguish between absolute energies, energy differences, and (usually one-photon, dipole-allowed) line intensities. Achieving a 0.1 % accuracy in variationally computed energies[56] is certainly feasible with potential energy surfaces (PES) computed at the highest levels of electronic structure

theory,[57] which translates to an average accuracy of 1–2 cm^{-1},[2] in the most interesting mid-infrared region. This accuracy is sufficient for unique assignment of experimental transitions with relatively high ($>10^{-26}$ cm $molecule^{-1}$) intensity, whose spectral separations are larger than the uncertainties of the first-principles line positions. However, spectral regions of highest interest today exhibit transitions with much smaller intensity and a much larger density, leading to a number of issues when experimental and computational results are to be used together. As to energy differences of rovibrational states with the same vibrational assignment, the computational accuracy could be much higher,[41,49,58] as most of the errors in the solution of a rovibrational Schrödinger equation is in the vibrational band origins, which cancel out during the subtraction. As to intensities, the computational uncertainty is considerably higher, nowadays it covers the range of 0.5–10 %, sometimes even better.[59] Nevertheless, this accuracy appears to be more useful than the 0.1 % accuracy of the absolute energies, as the intensities of closely-spaced spectral lines can be orders of magnitude different, helping the analysis and the assignment of observed features tremendously.[44]

There is another substantial difference between experimental and computed spectroscopic results one needs to emphasize[52–54] in order to understand some of the modern developments in the field of high-resolution molecular spectroscopy. While experiments provide much more accurate information than first-principles computations for systems containing more than a few electrons and nuclei, the relatively inaccurate theoretical information is much more complete (say up to the first dissociation limit). Completeness does not apply to experiments, which cover only a very small part of the transitions and the energy levels, even in the most thoroughly studied cases. To wit, note that for one of the spectroscopically most extensively studied polyatomic molecules, $H_2{}^{16}O$, the situation is still as follows (after 100 years of spectroscopic measurements leading to more than 200 publications): while the number of bound rovibrational states of $H_2{}^{16}O$ approaches one million, only about 2 %, that is about 20,000 energy levels have become known from experiment, and full coverage is available only up to 9000 cm^{-1},[23,60] while the first dissociation limit is above 40,000 cm^{-1}.[61,62]

Therefore, the practically most useful approach toward an improved understanding of high-resolution spectra is to combine all the information available, whether from experiments, empirical analyses, or computations. Indeed, composite line lists, utilizing all three types of spectroscopic

information, have become available for selected triatomic molecules, such as $H_2{}^{16}O$.[23,60] One should also add that strategies to combine experimental, empirical, and computed spectral data have been developed for slightly larger species, as well, see, for example, the BTRHE (Best Theory plus Reliable High-Resolution Experimental data) studies at NASA-Ames,[63–65] the ExoMol project at UCL,[7] and the TheoReTS (Theoretical Reims–Tomsk Spectral data) information system.[66]

This paper reviews, mostly from a historical perspective, the challenges and the advantages characterizing the joint application of experimental, empirical, and computational information during the analysis of spectroscopic data and the construction of line-by-line spectroscopic databases. The discussion is based mostly on research conducted by members of the Budapest group, often in collaboration with a number of experimentalists performing high-resolution and precision-spectroscopy measurements. The issues identified during the related research, some spelled out here *via* selected examples, lead directly to a set of recommendations, formulated at the end of this paper. The authors' hope is that these recommendations will help to improve the presentation of spectroscopic results, so that ambiguity concerning the data and the related metadata can be reduced or even diminished.

2. Issues with experimental data

Out of the many parameters characterizing each and every experimentally observable spectral feature, here we are concentrating on line positions and line assignments. The reason is that these are the quantities most directly linked to empirical and first-principles computed spectroscopic information.

2.1 Typographical errors

Since most of the experimental spectroscopic data are available only in a printed form (aggravated by the fact that often the original articles have been scanned in rather poor quality), there is a clear danger that some of the experimental information was typed in or became available incorrectly. This will remain a significant problem until all data are handled/reported fully digitally and all previously obtained data are either validated or refuted.

As an example, let us take a transition wavenumber from Ref. 67, whereby the authors ordered the measured positions of the assigned lines of $H_2{}^{16}O$ according to their increasing wavenumbers. As revealed during the creation of the W2024 database,[23] a line position out of this order, at 13,312.0013 cm^{-1}, possesses a MARVEL residual (*i.e.*, an observed minus MARVEL-predicted wavenumber deviation) of almost exactly 1 cm^{-1} (in fact, 0.9982 cm^{-1}). This round residual suggests that it is due to a typographical error in the position reported in Ref. 67.

It has been customary to publish experimental line positions only after they got labeled by a set of appropriate (good and approximate) quantum numbers, traditionally extracted from effective Hamiltonian (EH) fits. According to well-established quantum selection rules, there are certain symmetry requirements and highly limited changes in the rotational quantum numbers describing a transition. Violation of these selection rules leads either to a non-existent quantum state or a transition forbidden under the given experimental conditions. Before the advent of modern computers and data handling, the occurrence of typographical errors in the published data breaking selection rules was considered somewhat natural. However, even in newer data sources supplied with electronic appendices, there are lines reported with non-existing upper and/or lower states, as recognized, once again, during the compilation of the W2024 dataset[23,60] (see, *e.g.*, Ref. 68, listing 19 impossible quantum states).

2.2 Miscalibrations

Before the appearance of optical frequency combs,[70,71] the majority of high-resolution spectroscopic data came from Fourier-transform infrared (FT-IR) measurements. Being a relative frequency measurement technique, FT-IR positions are as good as the frequencies used for calibrating the lines. Thus, calibration of FT-IR spectra may have affected the reported positions much beyond measurement uncertainty, because the reference calibration frequencies applied in the calibration process may turn out to be somewhat inaccurate.

As an example indicating issues with the calibration of FT-IR sources, Fig. 1 reveals the presence of systematic errors in the transition wavenumbers reported in Ref. 69 concerning $H_2{}^{16}O$: most of the (red) MARVEL residuals, with respect to the original dataset, are concentrated on the positive part of the vertical axis, with a significantly positive median value. Relying on the MARVEL approach and the complete set of accurate data collected, one can straightforwardly find an optimized linear

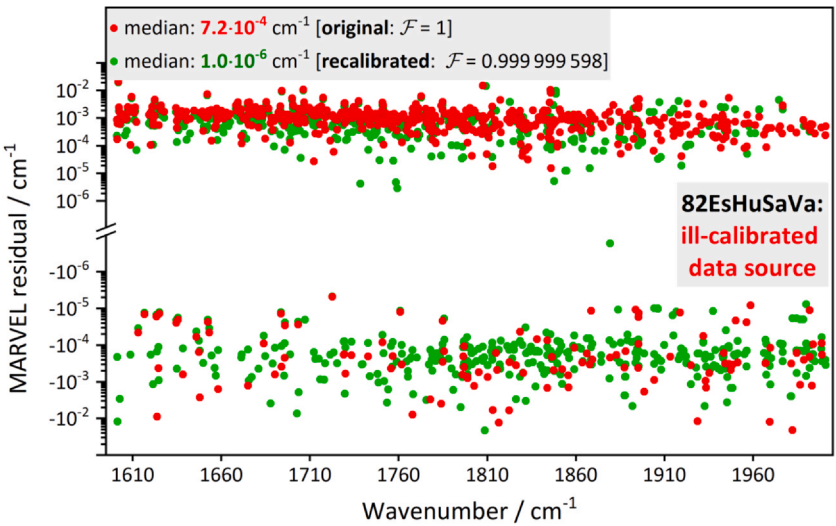

Fig. 1 Example showing the clear need for recalibration of a measured spectrum, using a linear calibration factor $\mathcal{F}$, as revealed during a MARVEL analysis of the rovibrational lines reported in 82EsHuSaVa.[69] For the convention how sources of experimental spectroscopic data are named, see Sec. 5.1.

recalibration factor, 0.999,999,598, for this source. Applying this factor to the experimental positions of Ref. 69, the new (green) residuals become distributed consistently on the positive and negative sides of the vertical axis, resulting in a negligible median deviation. One must mention that recalibration has a beneficial effect on the overall accuracy of the line positions given in Ref. 69, as well, reducing the median of the absolute residuals from 8.4×10^{-4} to 5.8×10^{-4} cm^{-1}.

2.3 Underestimated uncertainties

Unfortunately, it has been common practice in the high-resolution spectroscopy literature that the papers do not provide individual uncertainties for the parameters of the measured lines. Here we are concentrating on uncertainties of line positions, where the use of network-theoretical tools[55,72] helps to reveal problems with some of the reported values. Individual uncertainties provided by those measuring the spectrum often prove to be dependable: this is the case when all important uncertainty factors in the error budget are accounted for and the overlapping lines are treated properly, in accordance with peak heights, signal-to-noise ratios,

and spectral residuals. In contrast, reported average uncertainties, especially those corresponding to best-case scenarios, may be quite misleading.

The case shown in Fig. 2 uncovers an accuracy problem involving five far-infrared transitions observed for $H_2{}^{16}O$ between 118 and 480 cm^{-1} in five independent studies.[73–77] Four of these lines were supplied with individual uncertainties; the exception is the transition at 446.35 cm^{-1},[75] for which only an average uncertainty of 3×10^{-5} cm^{-1} is available. The lines form two four-membered cycles, called here 4-cycles, differing only in the green and red transitions in Fig. 2. The outer 4-cycle consists of lines with correct uncertainties, because its discrepancy is lower than its threshold (see the caption to Fig. 2 for the definition of these two quantities). The inner 4-cycle, however, is definitely problematic, with a 14 times higher discrepancy than the threshold (of course, the same holds for the red–green trivial cycle). Therefore, one may assume that this large

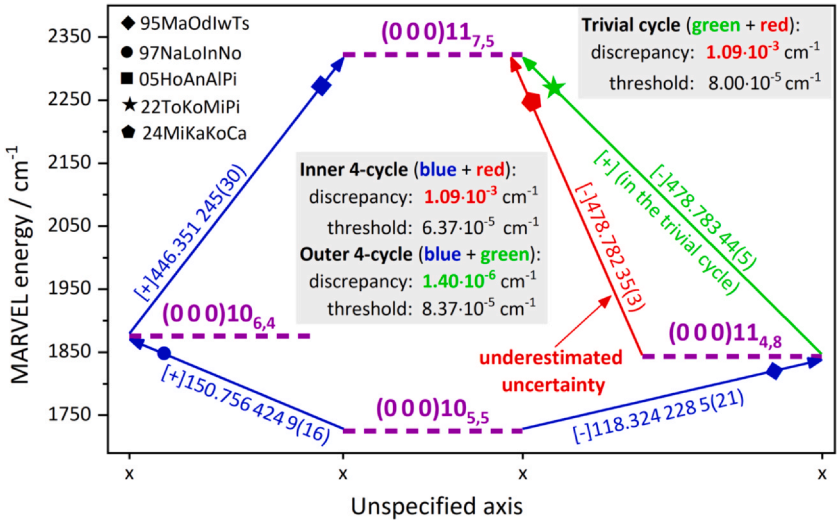

Fig. 2 Proof of an underestimated uncertainty for a line position, with evidence given by three cycles. The numbers on arrows are experimental wavenumbers in cm^{-1}, with the uncertainty of their last few digits in parenthesis, taken from 95MaOdIwTs,[73] 97NaLoInNo,[74] 05HoAnAlPi,[75] 22ToKoMiPi,[76] and 24MiKaKoCa.[77] For the naming convention of the sources, as well as the labeling of the quantum states, see Sec. 5.1. For all wavenumbers, signs are also given in brackets, which can be employed to determine the discrepancies (absolute sums of the signed positions) of the cycles. Notice that two signs are specified for the green line, because it changes sign within its trivial cycle. The discrepancies and the associated thresholds (sums of the wavenumber uncertainties), are given in the gray boxes.

discrepancy arises from the red transition shared by the two bad cycles. It turns out from Ref. 77 that (a) the red line is very weak in the spectrum recorded for a D_2O-enriched sample, (b) there is a strong $D_2{}^{16}O$ transition nearby, able to spoil the accuracy of the red line, and (c) the reported uncertainties are only statistical errors and do not include any systematic terms. As a result, the uncertainty of the red transition appears to be highly underestimated, and thus must be increased, by a factor of about 33, to at least 1×10^{-3} cm^{-1}.

2.4 Misinterpretation

The hardest problems with experimental data are related to the incorrect interpretation of measured spectral features, which might distort the numerical values of the retrieved line positions. Incorrect interpretation is due to an incorrectly assigned peak, causing incompatibility issues among the data in a global (MARVEL-like) treatment.

Although the reasons behind misassignments are quite diverse, they usually occur when (a) the labeling scheme applied for the underlying quantum states is ambiguous (for semirigid molecules this occurs at higher energies and excitations), (b) the closely-spaced transitions, producing overlapping line profiles, are not treated adequately (this information mostly comes from a source outside of the measurement and is usually unavailable to the experimentalist), and (c) "foreign" lines, belonging to contaminating species, appear in the recorded spectrum. A few examples for interpretation issues, all related to the spectrum of the $H_2{}^{16}O$ molecule, will be studied in detail in Sec. 5.2.

3. Issues with empirical data

Quantum theory offers several ways helping to interpret experimental rovibronic spectra. The most comprehensive and computationally most intensive one, the (quasi-)variational solution of the time-independent nuclear Schrödinger equation, is based on the full nuclear Hamiltonian. The strengths and weaknesses of this procedure will be discussed in Sec. 4. Here, two distinct approaches are dealt with: the first one is a Hamiltonian-free method relying solely on the Ritz principle,[18] while the second one uses a (highly simplified) effective Hamiltonian model. Both approaches provide a representation of the measured transition frequencies.

3.1 Issues with MARVEL energies

Hamiltonian-free approaches determine empirical energy levels from measured and validated transitions *via* line-inversion procedures.[19,78–83] The protocol and code we developed along these lines is MARVEL,[19–23] built upon the theory of spectroscopic networks.[55] MARVEL energies should be able to reproduce observed lines to experimental accuracy and, at the same time, provide transition frequencies not yet measured with an accuracy similar to that of the underlying measurements.

To gain a correct picture about the strengths and weaknesses of the MARVEL methodology, one must understand the limitations of network-based methods for the identification of outliers. During the analysis of spectroscopic networks, outliers are lines with incorrect wavenumbers, uncertainties, or assignments. As described in detail,[84] outlier-detection algorithms designed for SNs are built upon the presence of cycles and the notion of network (in)consistency. An SN is said to be consistent if the discrepancy is smaller than the threshold for each of its cycles, otherwise it is called inconsistent.

There are a few common misconceptions concerning outlier detection in high-resolution spectroscopy.[84] Perhaps the most unexpected one is connected to 'latent outliers', which cannot be recognized *via* network-theoretical tools, because they do not violate the consistency of SNs. Thanks to potential error cancellation in cycles, see misconception M5 in Ref. 84, in principle any line could be a latent outlier. In practice, a latent outlier is most frequently (a) a bridge or (b) a transition whose uncertainty is lower than the threshold in all of its cycles. For example, when a transition has an uncertainty of 10^{-4} cm^{-1}, but it takes part only in cycles with thresholds of 10^{-3} cm^{-1}, the accuracy of this line can be validated by MARVEL only to 10^{-3} cm^{-1}. This observation led to the concept of confidence intervals, introduced recently to MARVEL analyses.[23] A confidence interval value means a lower limit, below which no error can be revealed by MARVEL in a transition wavenumber or its uncertainty. For further details about confidence intervals, see Ref. 23.

Though the detection of outliers in spectroscopic networks is never a simple task, there are approaches which can help to uncover problematic lines destroying the accuracy of the derived energy levels and the predicted transition frequencies. In Ref. 84, a robust and efficient heuristic algorithm, called autoECART, was developed, standing for automatic Energy Conservation Analysis of Rovibronic Transitions.[84] autoECART is built upon

the investigation of network consistency by analyzing the properties of cycles in the spectroscopic network, yielding a collection of potential outliers (this contains, with high probability, all the outliers and only a minimal number of pseudo-outliers).

To increase the number of cycles in experimental spectroscopic networks, a useful approach is to include state-of-the-art computational data (*e.g.*, accurate first-principles energy differences) as artificial transitions. These additional data may help to make correct decisions in cases where there are conflicts among the transition wavenumbers, line assignments, and wavenumber uncertainties.

As emphasized above, incorrect entries may remain, even after the most elaborate checks, in the transitions dataset. Their detection requires new measurements, preferably with higher accuracy and better resolution. With all the advancement in experimental techniques, these certainly seem to be more and more feasible requirements. Furthermore, network-based design of experiments, advanced in our group,[41,85–87] can also assist in the selection of target lines for new (ultra)high-resolution spectroscopic experiments.[41,58,88–92]

3.2 Issues with effective Hamiltonian energies

The effective Hamiltonian models of high-resolution molecular spectroscopy contain a small set of effective spectroscopic parameters for each vibrational band of a given molecule, leading altogether to a large number of parameters when all the vibrational states are considered. The principal aim of EH fits is to reproduce measured line positions (and often intensities) within experimental accuracy. This process has traditionally antedated publication of the measurement results; in fact, often only these parameters and not the direct experimental line parameters were made available to the general public. When done successfully, the EH parameters obtained enable efficient interpolation within and a limited extrapolation beyond the actual measurements.

The spectroscopic literature contains a large number of examples discussing shortcomings of the EH approach. From the point of view of database developers, for example, a significant bottleneck in EH-based line-list generations is the lack of EH information about high-energy vibrational bands. The lighter the molecule, the higher the excitation, and the more complex the internal motions of the species under investigation, the more difficult it is to use the EH approach successfully, as exemplified by the case of the methanol molecule.[94,95] Here we discuss

only one breakdown concerning the EH method, found during our own analysis performed for the ground vibrational state of $^{14}NH_3$.[17]

Historically, spectroscopists considered[96–101] EHs not suitable for fitting to the observed high-resolution spectra of $^{14}NH_3$ to experimental accuracy. This assessment was due partly to the fact that the internal motions of ammonia are governed by a symmetric double-well inversion potential. Despite of these reservations, Pearson and co-workers[102–105] suggested that carefully constructed rotation-inversion EHs are able to describe the majority of the measured $^{14}NH_3$ lines with remarkable accuracy. In Ref. 17, we have identified problems with these EH fits: the predicted rotational energies deviated drastically, up to several cm^{-1}, from their MARVEL-based counterparts yielded in Ref. 17 for $^{14}NH_3$ (see the left panel of Fig. 3). These issues were traced back to the presence of floating components within the spectroscopic network of $^{14}NH_3$ transitions used during the EH fits, leading to correct line positions but erroneous EH energies. To overcome this apparent problem, that is to connect the floating components to the principal components, we decided to use a set of carefully selected artificial (first-principles) transitions, which vastly increased the accuracy of the deduced EH energy levels.

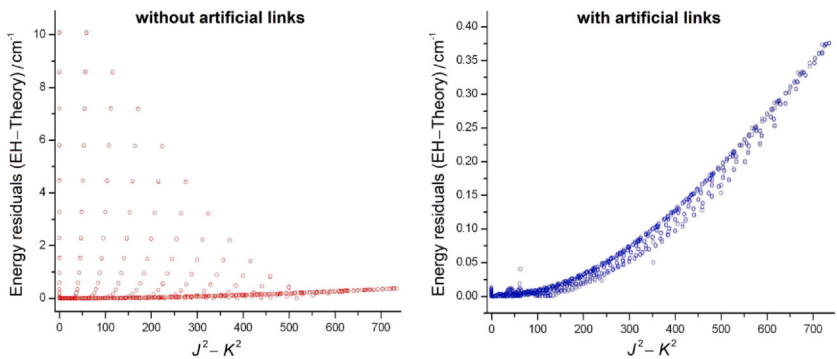

Fig. 3 Comparison of the effective Hamiltonian (EH) energies obtained for the ground vibrational state of $^{14}NH_3$ with their accurate first- principles counterparts taken from Ref. 93. The left and right panels, respectively, show the results produced without and with the addition of a few artificial (first-principles) transitions to the training set. These artificial lines were designed such that there remain no floating components in the spectroscopic network defined by the training set. Notice the very different vertical scale of the two panels. On the horizontal axis, *J* is the overall rotational quantum number, and *K* denotes the projection of the total angular momentum on the molecule-fixed axis *z*.

The presence of floating components is a general issue and of particular concern for systems characterized by restrictive selection or propensity rules. As illustrated for $^{14}NH_3$,[17] our combined theoretical and empirical approach results in accurate representation of both the observed transitions and the underlying rovibrational levels. Most importantly, the case of $^{14}NH_3$ proves beyond doubt that combining network theory and first-principles results during the calculation of EH parameters is a straightforward and useful approach, one which helps avoiding pitfalls associated with complicated EH models.

4. Status of first-principles computations

During the last two decades, it became increasingly realistic to use powerful (quasi-)variational methods, such as those relying on the discrete variable representation (DVR)[106–118] of the Hamiltonian of nuclear motions, to solve the related (time-independent) Schrödinger equation. These sophisticated techniques have allowed moving much beyond the traditional rigid-rotor–harmonic oscillator[119,120] and second-order vibrational perturbation theory[121–123] treatments of molecular vibrations and rotations. If the nuclear Schrödinger equation with an exact kinetic energy operator is solved in a variational fashion, the only significant approximation affecting the accuracy of the computed eigenenergies, besides the Born–Oppenheimer separation of nuclear and electronic coordinates,[124] is the use of *ab initio* computed PESs. The accuracy of these PESs, due partly to improvements in electronic-structure techniques and partly to the nearly exponential growth in available computer resources, improved tremendously over the years, making first-principles spectroscopic data significantly more dependable than just a decade ago.[56,115,125,126] Nevertheless, there is still a long way to go before first-principles computations will be able to produce energy levels with an accuracy approaching that of even the average of empirically-derived ones.

For the numerical solution of the time-independent nuclear (rovibrational) Schrödinger equation, several algorithms, together with associated codes, have been developed.[113,115–117,127–136] A particularly useful strategy has been programmed into the code GENIUSH (GEneral nuclear-motion code with Numerical, Internal-coordinate, User-Specified Hamiltonians),[116,117,136] developed in our group. The most important characteristics of GENIUSH are as follows: (a) it is a black-box-type code, such as most electronic-structure codes (the user needs to provide solely the internal

coordinates describing the motion of the nuclei and the potential/property surfaces), (b) it is applicable to any molecular system, any choice of recti- and curvilinear internal coordinates, and any embedding of the rotating axes (even the Eckart axis system can be used[137,138]), without the need to rewrite the essential parts of the code, (c) it accommodates any full- or reduced-dimensional model of a vibrating-rotating molecule even if it has an arbitrary number of versions,[139] thus it can treat not only semirigid but also quasis-tructural[140] molecules, (d) despite its reliance on the discrete variable representation, it has a built-in symmetry treatment,[136] and (e) it is able to compute a huge number of states through the use of variants of iterative (partial) diagonalization techniques.[141]

In general, with the aid of first-principles nuclear-motion methods, it has become possible to compute a very large number of quantum states for polyatomic molecules, even for cases with extremely complex nuclear dynamics.[136,140,142–144] In particular, all of the bound vibrational states of triatomic species,[145,146] and some of the resonance states,[147] that is states above the first dissociation limit of the molecule, can be computed, making them amenable for spectroscopic characterization. Along with symmetry classification, the approximate vibrational and rotational labels one can attach to rovibrational states[148] are much needed for the correct interpretation of spectroscopic experiments. As detailed in Ref. 56, the nuclear-motion wave functions computed give a clear indication about the extent of state mixing, which could also become important when setting up EH models for the representation of experimental spectroscopic results.

To some extent, first-principles computations deliver information complementary to that of empirical approaches. This complementary nature is depicted in Fig. 4, where (a) the observed, (b) the MARVEL-predicted but unobserved, (c) all the observed plus the MARVEL-predicted, and (d) the complete set of variational results are plotted for $H_2{}^{16}O$ in four separate panels, employing the records of our CW2024 composite line list.[23,60] As obvious from Fig. 4A, there is a definite intensity bottleneck for the measured transitions: under a certain intensity cutoff, say 10^{-26} cm molecule^{-1}, only few lines have been observed. This intensity issue does not appear in the predicted line list based on empirical (MARVEL) energies, yielding considerable coverage even at very low intensities (see Fig. 4B). Forming a combined set from the observed and the MARVEL-predicted transitions, see Fig. 4C, reveals that the observed lines contain lot more information than their measured positions. Nevertheless,

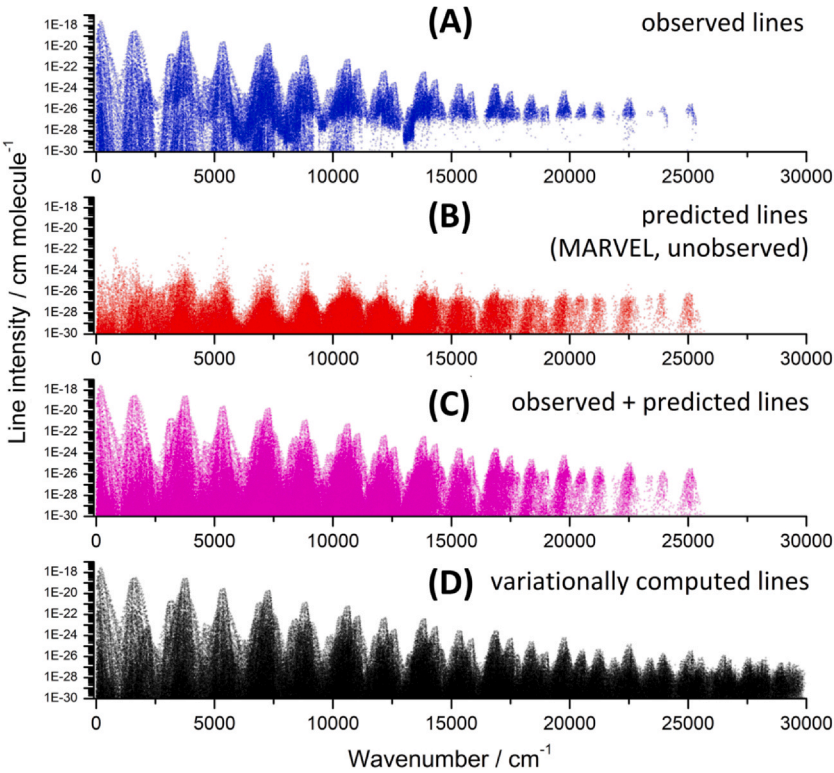

Fig. 4 Comparison of experimental, empirical, and variational line lists, up to 30,000 cm^{-1}, obtained for the $H_2{}^{16}O$ molecule. The transitions displayed in this figure correspond to one-photon dipole- allowed absorption lines, with intensities related to 296 K. The data behind this figure were taken from Ref. 23, utilizing the first-principles results of Ref. 149.

at large wavenumber values even the observed plus predicted dataset is far less complete than the variational line list, as shown in Fig. 4D.

While the absolute accuracy of first-principles computed energies is relatively limited,[41,49,58,150] the uncertainties of energy differences can be much lower, and in some cases they are able to compete even with the accuracy of precision-spectroscopy measurements.[41,58] Fig. 5 gives a graphical illustration of GENIUSH-computed energy splittings, obtained in Ref. 58, between some close-lying *ortho*- and *para*-$H_2{}^{16}O$ states with the same vibrational assignment (note that the *ortho*/*para* nuclear-spin isomers arise as H is a spin-1/2 nucleus, whereas ^{16}O has zero spin).[139,151] These splittings and their uncertainty bars, respectively, correspond to the

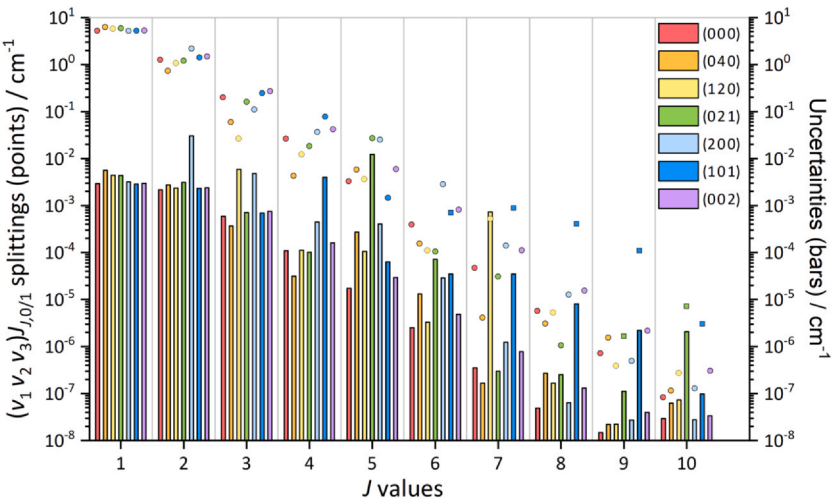

Fig. 5 Variationally computed $(v_1\ v_2\ v_3)J_{J,0/1}$ splittings, up to $J = 10$, for various vibrational bands of $H_2{}^{16}O$ (see Sec. 5.1 for the rovibrational labeling convention). The points corresponding to the splitting values are related to the left vertical axis, while the bars illustrating the splitting uncertainties are plotted on the right vertical axis (for the numerical results behind this figure, see Ref. 58). The vibrational states are distinguished by their colors given in the top right corner of this figure. For splittings with dots, the $K_c = 0$ energy is higher than its $K_c = 1$ pair, while for those with squares, the converse relation is satisfied.

averages and the standard deviations of the results produced with multiple PESs and basis sets (these estimates proved to be realistic, verified by precision-spectroscopy measurements[41,58,88,89,91,92]). Fig. 5 suggests that most of the uncertainties are orders of magnitude smaller than the unsigned splittings, due to cancellation in the vibrational errors. However, there can be problematic cases, like the yellow dot/bar pair at $J = 7$ in Fig. 5, where a relatively large amount of uncertainty appears in the computed splitting. Such occurrences indicate particularly strong resonances among closely-spaced interacting states, an issue reducing the accuracy of such perturbed energy splittings.

In the fourth age of quantum chemistry,[56] there remain several significant challenges which need to be overcome to advance computational spectroscopy further: (a) construction of fully global and accurate PESs for many-electron systems, without reliance on empirical refinements (at present, the prospects appear to be somewhat bleak[126]); (b) use of machine learned PESs[144,152] instead of those fitted with a given functional form; (c) performing converged variational nuclear-motion computations

close to (just below and above) the dissociation asymptotes for polyatomics; (d) handling of nonadiabaticity and post-Born–Oppenheinmer effects, as well as cases with multiple surfaces; and (e) effective extension of accurate nuclear-motion computations to higher dimensions and excitations.

5. Resolving complex spectral issues

The previous sections were mostly devoted to the description of the individual strengths and weaknesses characterizing experimental, empirical, and computational spectroscopic results, which can be used during the interpretation of high-resolution molecular spectra. The weaknesses mentioned mean that line lists available at present in the literature contain an unidentified number of problems, which usually surface when new measurement results become available. It is our strong belief that the detective work leading to the realization of these problems and the eventual solution of the issues uncovered require the joint utilization of all available information. After some preliminary remarks, a couple of specific spectral problems will be presented with feasible solutions, demonstrating the utility of the joint approach advocated.

5.1 Preliminary remarks

The data behind the examples provided in the upcoming Sec. 5.2 concern the parent water isotopologue, $H_2{}^{16}O$, and come from our recent W2024 investigation[23,60] of its rovibrational spectra. To begin with, we introduce the conventions necessary to understand these examples and their spectral illustrations (Figs. 6–13).

In what follows, a number of spectroscopic data sources will be referenced in the form of so-called tags. Adopting a convention defined in Ref. 36, a tag is formed by the last two digits of the publication year, followed by the first two characters of the authors' surnames up to the first four authors (for "special" references, like one-author sources and those with ambiguous tags, our established convention contains further rules, but they are not relevant here).

The (rovibrational) states of $H_2{}^{16}O$ are labeled as $(\nu_1\ \nu_2\ \nu_3)J_{K_a,K_c}$, where ν_1, ν_2, and ν_3 are the normal-mode quantum numbers of the symmetric stretch, bend, and antisymmetric stretch motions, respectively, J is the overall rotational quantum number, while K_a and K_c symbolize the traditional prolate- and oblate-top rotational quantum numbers, respectively.[119,120,153]

Moreover, $(v_1' \, v_2' \, v_3')J'_{K_a',K_c'} \leftarrow (v_1'' \, v_2'' \, v_3'')J''_{K_a'',K_c''}$ designates a rovibrational transition, where $'$ and $''$ distinguish between its upper and lower states, respectively.[153] When two transitions share the same upper state, they will be referred to as a Λ pair. If two or more lines are closer to each other than can be resolved by a specific experiment, they form what will be called an unresolved multiplet (a multiplet of two transitions will be simply termed a doublet).

The *para*/*ortho* states of $H_2{}^{16}O$, specified by $(-1)^{v_3+K_a+K_c} = +1/-1$, pertain to its two nuclear-spin isomers. Since symmetry forbids *ortho* ↔ *para* transitions,[139,154] these lines possess extremely low one-photon absorption intensities, which so far has prevented their observation in experimental high-resolution spectra. If two states differ solely in either their K_a or K_c values, they will be considered an *ortho–para* pair. When U_1/U_2 and L_1/L_2 mean *ortho–para* state pairs, the transitions $U_1 \leftarrow L_1$ and $U_2 \leftarrow L_2$ will be handled as *ortho–para* complements of each other, where U/L refers to upper/lower state.

In our spectral analyses, the experimental line positions/intensities will be compared to their predicted counterparts. The predicted intensities will be taken from HITRAN,[4] whereas the wavenumber predictions will be obtained from combination-difference (CD) relations. For a transition pair indexed with (i, j), two forms of CDs will be used as wavenumber predictions:

$$\sigma_j^{\text{pred}} = \sigma_i + E_{\text{low}(i)} - E_{\text{low}(j)}, \tag{1}$$

if (i, j) represents a Λ pair, or

$$\sigma_j^{\text{pred}} = \sigma_i - \rho_{ij}^{\text{pred}}, \tag{2}$$

when an accurate relative position, ρ_{ij}^{pred}, is available for the (i, j) pair. In these formulas, (a) the σ_i value is obtained from experiment, (b) the lower-state energies, $E_{\text{low}(i)}$ and $E_{\text{low}(j)}$, come from the W2024 energy list,[23,60] while (c) the ρ_{ij}^{pred} value is expressed as

$$\rho_{ij}^{\text{pred}} = d_{ij}' - d_{ij}'', \tag{3}$$

where the (signed) splitting of the upper/lower states, d_{ij}'/d_{ij}'', is derived from variational BT2[155] and/or POKAZATEL[149] energies (see also Eq. (3) of Ref. 23). As emphasized in Sec. 4, under favorable conditions these variational energy splittings may have high accuracy, and their uncertainties

can be estimated through differences between the BT2 and POKAZATEL results (as a reasonable uncertainty estimator, see Eq. (4) of Ref. 23).

Next, the extensive set of rules applied during the construction of the spectral illustrations, Figs. 6–13, is discussed. In these figures, the primary/secondary issues are presented with red/yellow boxes, supplied with red/yellow comments. The other colors indicate rovibrational assignments, POKAZATEL line separations (*i.e.*, unsigned relative positions), and peaks modeled *via* Voigt profiles. These spectral profiles utilized (a) the positions/intensities of the observed peaks, whose sources are given by the colors of the simulated profiles, (b) the 296 K Doppler half width as Gaussian width, and (c) 800 kHz[156] as Lorentzian width. The peaks studied are distinguished with unique identifiers, **P***n* ($n = 1, 2, 3, \ldots$), whose colors are matched with the most reasonable peak assignments. The vertical axis of each spectral figure represents the intensity on a logarithmic scale, whereas the horizontal axis shows the experimental transition wavenumbers as axis values, often with several axis breaks.

To aid the comparison of different spectral interpretations, sticks linked with symbols are used. For a particular stick, (a) its color corresponds to a rovibrational assignment, (b) its height means a HITRAN intensity scaled with terrestrial abundance, (c) its position represents a measured or a CD-predicted wavenumber, depending on whether its symbol is filled or empty, respectively, (d) the shape of its symbol specifies the data source delivering its position (directly or *via* CD relations). When, for example, the wavenumber of transition t_1 is predicted from that of t_2, this is designated with a dash-dotted arrow, whereby the shaft and the head inherit the colors of t_1 and t_2, respectively. Finally, note that (a) a bi-colored dashed marker joins two transitions attached with a POKAZATEL separation, (b) a skew dotted arrow signifies an experimental upper-state energy correction, and (c) the assignments of some line pairs are given in the same row with slashes for compactness.

5.2 Selected examples

In this subsection, seven problems with the interpretation of spectral features, given in Figs. 6–13, are discussed and resolved. The examples chosen involve low-intensity ($S < 10^{-26}$ cm molecule^{-1}) transitions measured with cavity ring-down spectroscopy (CRDS) setups[67,157–159] in the near-infrared and visible regions. In this wavenumber and intensity regime, the $H_2{}^{16}O$ lines are rather densely spaced, aggravating their correct

interpretation, especially when (a) a line is not part of measured cycles, (b) there are contaminant components yielding "foreign" transitions in the sample, and (c) sometimes the theoretical intensities are of insufficient accuracy.[160,161] Nevertheless, as presented below, the application of accurate BT2/POKAZATEL relative positions helps to choose the best spectral interpretations even in complicated cases.

5.2.1 Incompatible Λ pair

Fig. 6 presents a case where two sources of experimental transitions published by the same authors, 21VaMiCa[157] and 22VaMiCa,[158] are in conflict with each other through a Λ pair formed by the blue and magenta transitions. The intensity and the position of the magenta *ortho* line, under peak **P2**, can be confirmed straightforwardly: the position is fully supported by the olive POKAZATEL separation from its brown *para* counterpart. Hence, the issue is with the blue line under **P3**. This apparent conflict can be reconciled by assigning the green transition of Fig. 6, instead of the blue one, to peak **P3**. Then the remaining question is why there is no line reported in 22VaMiCa[158] on the left-hand side of **P3**, where the magenta transition predicts the blue one. A personal communication[162] suggests that

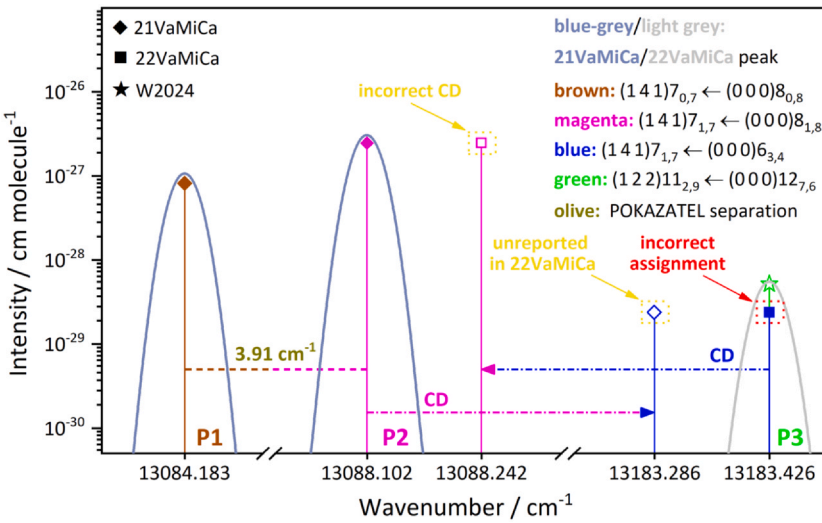

Fig. 6 An incompatible Λ pair, with line positions utilizing from data sources 21VaMiCa,[157] 22VaMiCa,[158] and W2024.[23,60]

the blue line is indeed at 13,183.286 cm^{-1} in the spectrum, whose position has not been reported in the source 22VaMiCa.

5.2.2 Misinterpreted foreign peak

As seen in Fig. 7, a recent source, 23KoMiKaCa,[159] interprets the peak **P6** as an unresolved (dark cyan) doublet of a $HD^{16}O$ (cyan) and a $H_2{}^{16}O$ (green) line. In fact, this interpretation was inherited from 15CaMiLoKa,[165] where the $(0\,5\,1)5_{1,5}$ energy, using an emission line of 05CoBeCaCo,[163] was adopted from the Ref. 38. While the position of peak **P6** agrees within 2×10^{-4} cm^{-1} in 15CaMiLoKa and 23KoMiKaCa, its intensity is four times higher in 15CaMiLoKa than in 23KoMiKaCa. The intensity discrepancy between the two sources must be due to a perturbing $^{14}NH_3$ line, blue-shifted by 0.04 cm^{-1} from **P6**, whose intensity is 18 times larger in 15CaMiLoKa than in 23KoMiKaCa, and 37 times greater than the 23KoMiKaCa intensity of peak **P6**. Relying on the perturbed 15CaMiLoKa intensity of peak **P6**, it seemed reasonable that **P6** also covers the green transition.

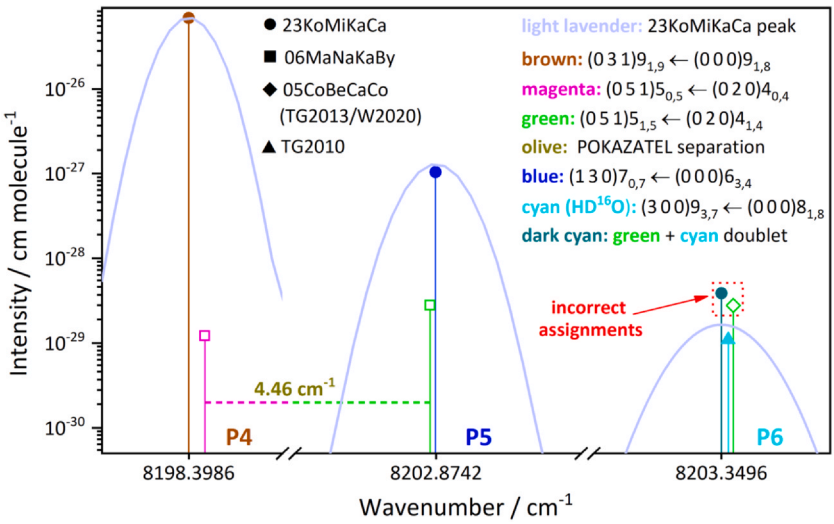

Fig. 7 Misinterpreted foreign peak (**P6**). The data sources of the transition wavenumbers are 05CoBeCaCo,[163] 06MaNaKaBy,[164] TG2010,[37] TG2013,[38] W2020,[42] and 23KoMiKaCa,[159] whereby "TG" means that the results were generated by an IUPAC task group on "A Database of Water Transitions from Experiment and Theory" (Project No. 2004–035-1–100).

Nevertheless, considering the 23KoMiKaCa intensity of peak **P6**, as well as the magenta (**P4**) and green (**P5**) predictions deduced from two well-resolved 06MaNaKaBy[164] lines around 11,350 cm^{-1}, the situation changes significantly. As the difference of the two 06MaNaKaBy predictions is entirely corroborated by the POKAZATEL-based line separation, this suggests that the green $H_2{}^{16}O$ transition is not under peak **P6** but under peak **P5**. Furthermore, placing just the cyan $HD^{16}O$ line under peak **P6** also resolves the anomaly between the observed and the reference HITRAN intensities: their relative deviation reduces to 33 %.

5.2.3 Erroneous assignment of an ortho–para doublet

Fig. 8 depicts the case of a well isolated, but misassigned doublet of an *ortho* (magenta) and a *para* (brown) line pair. The source 21VaMiCa[157] links the brown line to peak **P7**, whose position disagrees with the corresponding POKAZATEL separation. To reconcile the problem, the brown line should be placed under peak **P8**, a blue-shifted peak which was left unassigned in 21VaMiCa.[157] With this alternative choice, the upper-state splitting determined from these lines will have an appropriate sign and magnitude (see the upper-right corner of Fig. 8). One can assign **P7**, as well, using the green line with a consistent HITRAN intensity.

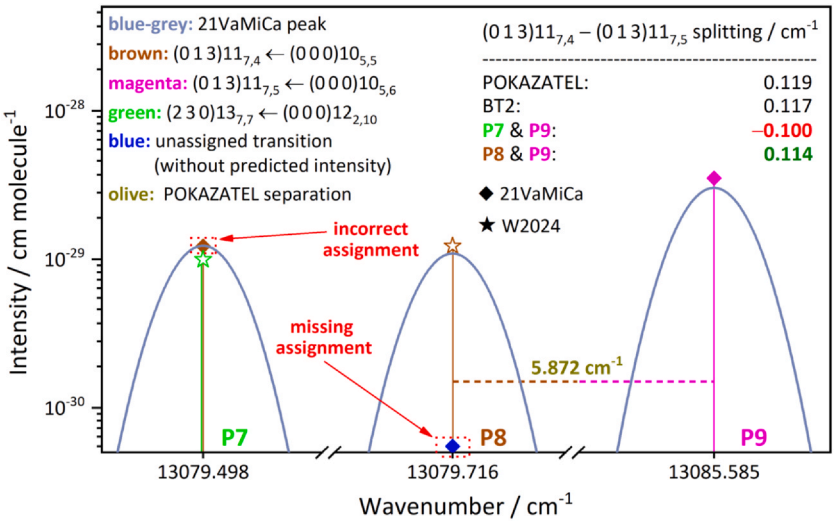

Fig. 8 Erroneous assignment for an *ortho–para* doublet of $H_2{}^{16}O$. The data sources of the transition wavenumbers and energy-level splittings are BT2,[155] POKAZATEL,[149] 21VaMiCa,[157] and W2024.[23,60]

5.2.4 Unrecognized perturbing line

The case displayed in Fig. 9 involves five transitions, three of which are associated with the same upper state. For the wavenumbers of these three lines, the W2020-$H_2{}^{16}O$ dataset[42] contains empirical estimates, which were derived from the **P12** position given in 08CaMiLi.[166] Subsequently, the first two authors of 08CaMiLi[166] published another paper, 21VaMiCa,[157] in which they claimed that they had corrected the W2020 wavenumber of the green transition by ≈ 0.02 cm^{-1}, thereby correcting the W2020 upper-state energy of this line. It was not mentioned in 21VaMiCa, however, that this large shift was induced by the **P12** peak of their older source, 08CaMiLi.[166] In spite of this sizable energy shift, the uncorrected W2020 wavenumber was still listed in 22VaMiCa[158] as a recommended position for the magenta transition. Obviously, the magenta line must be near the center of the **P11** peak, almost fully coinciding with the more intense brown transition. In their latest study,[167] the authors recognized this issue and eliminated the incorrect prediction, 13,396.4275 cm^{-1}, from their recommended line list. The reason behind the inaccuracy of peak **P12** can be the presence of a close (cyan) transition in the spectrum, which is supported by a reanalysis of peak **P12**.[162] Refitting **P12** as a line doublet yields 13,444.202 and 13,444.251 cm^{-1} for

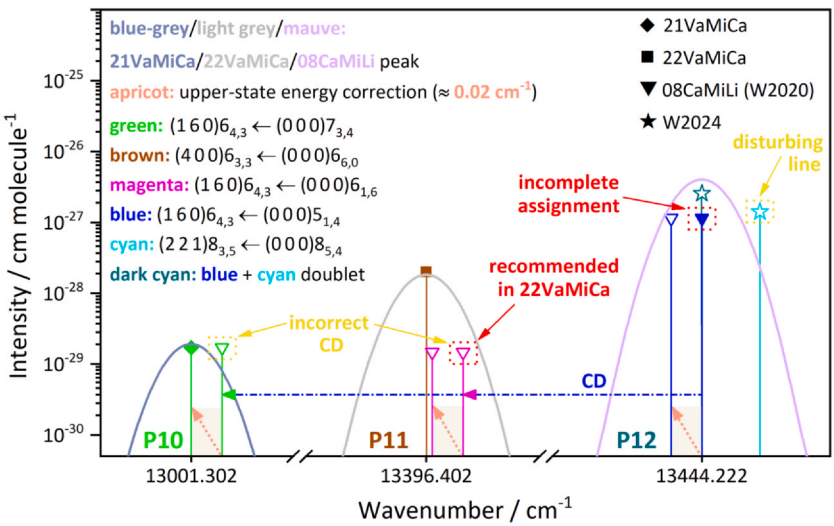

Fig. 9 Unrecognized perturbing line. The data sources employed are 08CaMiLi,[166] W2020,[42] 21VaMiCa,[157] and 22VaMiCa.[158]

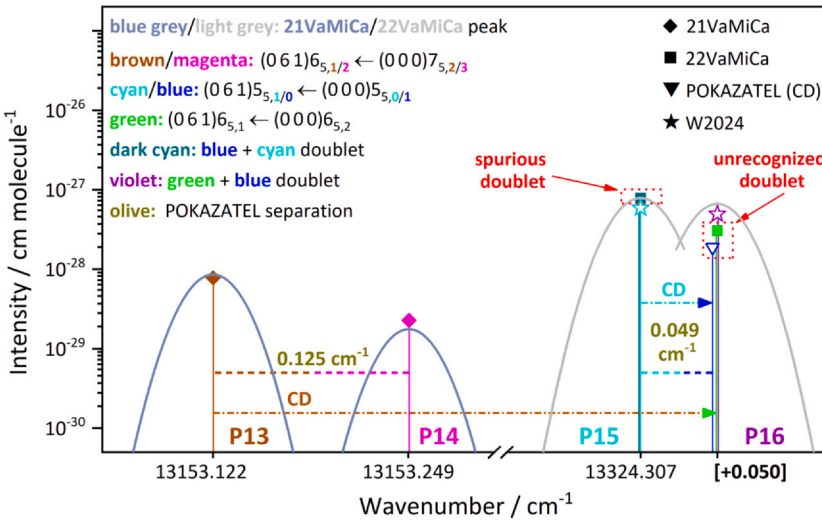

Fig. 10 Confused nearby lines. The data sources utilized are POKAZATEL,[149] 21VaMiCa,[157] 22VaMiCa,[158] and W2024.[23,60]

the positions of the blue and cyan transitions, respectively,[162] in fairly good agreement with their predicted wavenumbers.

5.2.5 Confused nearby lines

Fig. 10 demonstrates a problem related to two nearby peaks, **P15** and **P16**. In the interpretation given by 22VaMiCa,[158] **P15** covers the blue and the cyan lines as an unresolved (dark cyan) doublet, while only the green transition resides under **P16**. Position of the green line is endorsed by the brown/magenta pair under **P13**/**P14**. To comply with the POKAZATEL relative position of the cyan/blue pair, the blue transition should be at roughly + 0.049 cm^{-1} away from the cyan one. Thus, **P15** is not a cyan/blue doublet, as its blue line must be under **P16**.

5.2.6 Misuse of first-principles data

Fig. 11 illustrates how a first-principles Λ pair can be misused, as exemplified by peaks **P17** and **P18** assigned in 21VaMiCa[157] and 22VaMiCa,[158] respectively. 21VaMiCa tied the brown POKAZATEL line to **P17**, imposing a correction of around + 0.2 cm^{-1} on its position and hence on its upper-state energy. To remain consistent, the same correction should have been applied to the blue POKAZATEL transition. This indicates that if the brown line is around **P17**, the blue transition (triangle) cannot be

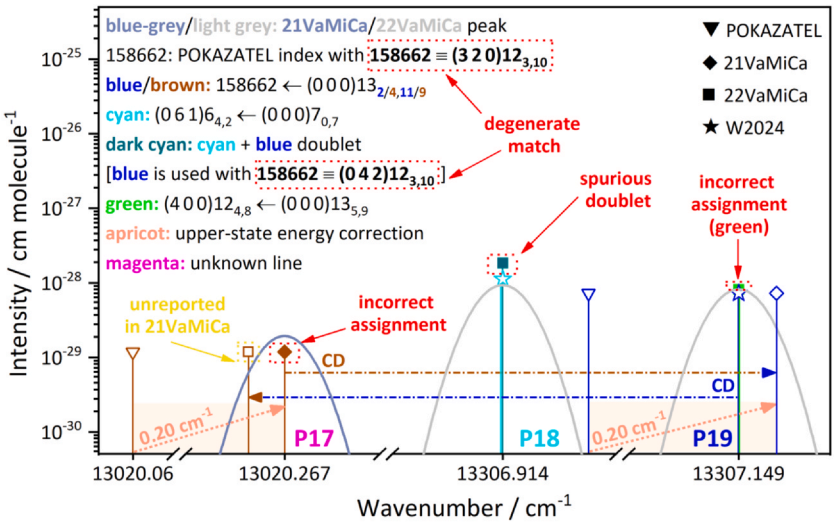

Fig. 11 Misuse of first-principles data. The data sources used are POKAZATEL,[149] 21VaMiCa,[157] 22VaMiCa,[158] and W2024.[23,60]

near peak **P18**. In contrast, the "phantom" blue line at **P18** has been attached to **P18** in 22VaMiCa,[158] although not with the same upper-state vibrational parent as that of the brown transition. However, **P18** has nothing to do with the blue line, leaving only the cyan one under **P18**.

If peak **P17** was indeed due to the brown line, there should be a hint of the blue transition, shifted away by $+0.03$ cm^{-1} from **P19**, but this additional peak is absent from the measured spectrum.[162] There exists, however, an unreported peak,[162] shifted away by -0.03 cm^{-1} from **P17** with appropriate intensity, which proves that the blue transition is located at peak **P19**. In this case, the green line cannot be at **P19**, because the blue/green doublet intensity is incompatible with the observed value, as well as with the first-principles relative position of the violet/green doublet displayed separately in Fig. 12. For peak **P17** of Fig. 11, no reasonable assignment could be found.

5.2.7 Systematic misassignment

Fig. 13 documents a complex assignment conflict, affecting three peaks with very similar position and intensity, namely **P23**, **P24**, and **P25**. In this example, it was quite difficult to uncover the relationships among the mislabelled lines. In the end, it became clear that one can compose three

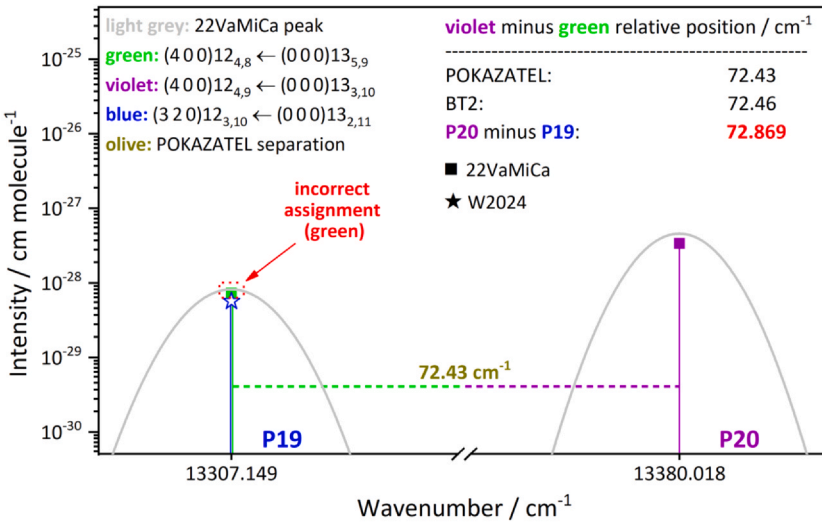

Fig. 12 Auxiliary figure to Fig. 11. The data sources applied are BT2,[155] POKAZATEL,[149] 22VaMiCa,[158] and W2024.[23,60]

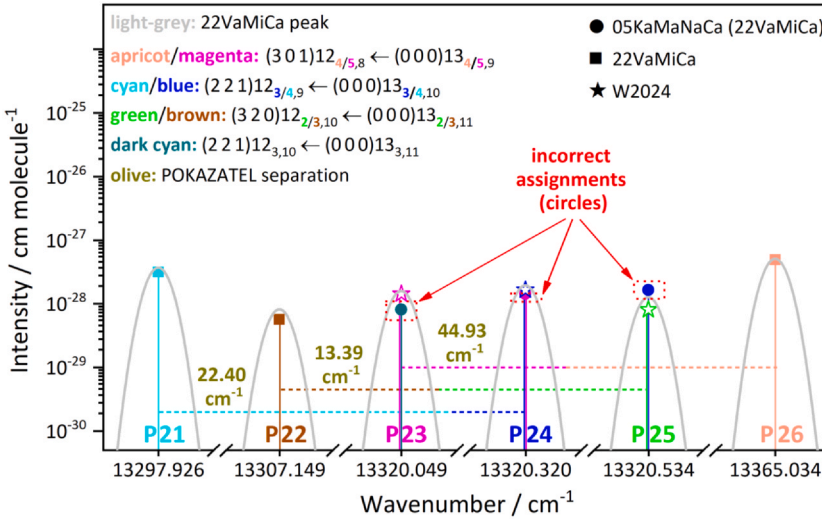

Fig. 13 Systematic misassignment. The data sources employed are 05KaMaNaCa,[67] 22VaMiCa,[158] and W2024.[23,60]

transition pairs, that is brown–green, cyan–blue, and apricot–magenta pairs, whose second members yield the correct assignments for peaks **P23**–**P25**. The separations of the resulting pairs are reproduced quite well, within 0.01 cm^{-1}, by first-principles (POKAZATEL) predictions.

6. Summary and recommendations

Based on the past and present situation of the field of high-resolution (and precision) spectroscopy, a number of recommendations can be formulated helping to minimize the extent of data conflicts when experimental, empirical, and computed data, separately considered to be dependable, are available. It is suggested that if these recommendations were followed by workers in the field more or less closely, the most striking conflicts among the different data would disappear or could be handled and knowledge generation concerning complex spectra of molecules would become significantly more streamlined.

First, we must stress that the quality, the accuracy, and the utility of data from the three types of data sources (experimental, empirical, and computational) can only be compared in a meaningful way if all the data and the associated codes used for their determination become publicly available to all those who desire to perform such comparisons. Thus, a perhaps simple, but admittedly hard to follow, recommendation is that the FAIR (findable, accessible, interoperable, reusable) principle[168] must be followed in spectroscopic studies. Unfortunately, this principle has rarely been applied in its full sense in high-resolution molecular spectroscopy, causing a number of issues, some mentioned in Secs. 2 and 5. Compliance with the FAIR principle should be checked, as closely as possible, by editors of journals publishing the results of such studies.

In the past, providers of high-resolution spectroscopic data may not have been able or willing to share their actual spectra, just their representation *via* a limited number of spectroscopic (mostly effective Hamiltonian) parameters (see Sec. 3). Under these circumstances, these usually high-quality data should be considered to be "lost" to the community,[169] in particular to database builders and users. Consequently, our second recommendation is that full information about the lines and, whenever feasible, perhaps even the experimental spectra with proper metadata, should be published and made available to interested readers, like it has been done recently for two $H^{16}OCl$ isotopologues.[44] Besides open access to experimental recordings of spectra and the related metadata, in many cases detailed information concerning the best spectral fits might also prove helpful. This would require to make the fitting codes available, as it was done with SPFIT[170] and PGOPHER[171] (needless to say, the accompanying input files used to run these codes can also be highly valuable).

When reporting measured rovibrational lines, all of the spectral parameters, including positions, intensities, widths, and shifts, should be

supplemented with conservative individual uncertainties. Knowing these uncertainties is extremely important, as measured spectra depend critically on a number of conditions, including composition, pressure, and temperature. Estimating reasonable individual uncertainties is a task most suited for experimentalists publishing measured lines; thus, this is our third recommendation. If providing line-by-line uncertainties is not feasible for some reason, at least transitions having uncertainties significantly worse than the average should be clearly indicated. Reporting only best-case uncertainties, with little or no indication as to which lines they apply to, cannot be regarded as a good practice. In many publications where individual uncertainties are not given, the authors provide observed – calculated (EH) values, which could indicate a problem with the measured line position. Unfortunately, without detailed information about the spectrum and the fitting, it is difficult to determine whether the calculated or the measured line position is incorrect.

It happens, more often than desirable, that the same experimentalists, over years of valuable studies, introduce new experimental datasets, which often contain improved estimates for their previous experimental results. This is highly useful and desirable, except when the old records remain uncorrected and there are unmentioned conflicts between the old and the new measurement results. It could be difficult to trace such hidden problems, especially when the measured spectra, the spectral parameters, or the line-profile fits are unavailable. Thus, our fourth recommendation is that when reporting their new results, with most likely improved resolution and better accuracy, experimentalists should go over their old results and point out, one by one, all conflicts. Of particular concern is that through a spectroscopic-network approach all measurement results become connected and the new measurements may affect line parameters in regions outside of the actual measurements.

Efficient treatment of tens if not hundreds of thousands of spectral features, leading to self-consistent databases, is an important and extremely timely problem of today's high-resolution (and precision) spectroscopy. Accurate and self-consistent datasets are demanded by developers and users of spectroscopic information systems, like HITRAN[4] and ExoMol.[8] The reliability of the end results yielded by empirical methods, like the entries of the (C)W2024 database,[23] critically depend on the correct interpretation of the underlying ("input") experimental data. This is especially true when the input data come from many different sources, measurement techniques, and research groups. Incorrect assignments and/or underestimated initial uncertainties may have a

significant distortion effect on the empirical energies derived and the line positions predicted, hindering their utilization in modeling studies. The MARVEL code, which is accessible in an online form on the MARVELOnline webpage, may assist the work of both data providers and database builders when their goal is to detect and resolve consistency problems.

As evident from this study, as well as from many similar ones, both experimental and computational spectroscopists must be careful when comparing their results of vastly different virtues and weaknesses. For instance, if the experimental data and metadata, including the measurement conditions and the uncertainties of the line parameters are not shared in full, one cannot expect that database builders will be able to pick the best measurement(s). While experiments can easily produce data with an accuracy exceeding those of first-principles computed results by several orders of magnitude, only theory can come up with an exhaustive, preferably complete, list of transitions under the given experimental constraints. Thus, it is particularly important and advisable to match the measured lines with their computed/empirical counterparts. It would also be highly useful if such comparisons would result in a common set of standardized interpretations, assignments and labels, for the lines, accepted and followed by the community, guiding future, ever more accurate experimental, empirical, and computational studies.

As to theory, it is important to provide access to both the codes and the associated data and metadata, such as potential energy and property (*e.g.*, dipole moment) surfaces, upon which the simulation of a spectrum is based. The computations performed should be fully specified; for example, it is not uncommon for papers to omit stating whether atomic or nuclear masses have been used during the solution of the nuclear Schrödinger equation (resulting in particularly large differences for molecules containing light elements, most importantly hydrogen). There exists, in the atomic and molecular physics community, an almost decade-old recommendation[172] that computed data, claimed to be "accurate", should include uncertainty quantification. Thus, the results of accurate first-principles computations of rovibronic energy levels and spectra should be accompanied by uncertainty estimates based on an as complete uncertainty budget as feasible. As shown repeatedly, there is considerable need for highly accurate estimates of energy splittings of close-lying rovibrational states, whose uncertainties could be obtained, for example, through the use of various basis sets and potential energy surfaces, upon which the precision and the accuracy of the results coming from the

solution of the nuclear Schrödinger equation are based.[41,58] Similar arguments hold for the computation of Einstein-*A* coefficients and the related transition intensities.[173]

It is the sincere hope of the authors that the above recommendations will be considered by all parties, sparking a renewed conversation among experimental spectroscopists, designers of empirical treatments, theoreticians computing high-resolution spectra, and developers of spectroscopic information systems. Such conversations would be definitely advantageous for all those involved and for the scientific and engineering communities relying on accurate spectroscopic information.

Acknowledgments

This work was supported by NKFIH (grant no. K138233 to AGC and grant no. PD145972 to RT). Dr. Semen N. Mikhailenko is thanked for fruitful discussions, as well as for his cordial assistance in checking different assignment options in the observed spectra of Refs. 157, 158, and 166. The authors are also grateful to Dr. Georg Mellau for useful comments on the manuscript.

References

1. Quack, M.; Merkt, F. (Eds.); *Handbook of High-Resolution Spectroscopy;* Wiley: Chichester, 2011.
2. Polyansky, O. L.; Császár, A. G.; Shirin, S. V., et al. High-Accuracy *ab Initio* Rotation-Vibration Transitions for Water. *Science* **2003,** *299*, 539–542.
3. Merkt, F.; Quack, M. Molecular quantum mechanics and molecular spectra, molecular symmetry, and interaction of matter with radiation. In *Handbook of High-Resolution Spectroscopy;* Quack, M., Merkt, F., Eds.; Wiley: Chichester, 2011; pp. 1–55.
4. Gordon, I. E.; Rothman, L. S.; Hargreaves, R. J.; Hashemi, R.; Karlovets, E. V.; Skinner, F. M.; Conway, E. K.; Hill, C.; Kochanova, R. V.; Tana, Y.; Wcislo, P.; Finenko, A. A.; Nelson, K.; Bernath, P. F.; Birk, M.; Boudon, V.; Campargue, A.; Chance, K. V.; Coustenis, A.; Drouin, B. J.; Flaud, J.; Gamache, R. R.; Hodges, J. T.; Jacquemart, D.; Mlawer, E. J.; Nikitin, A. V.; Perevalov, V. I.; Rotger, M.; Shines, K. P.; Tennyson, J.; Toon, G. C.; Tran, H.; Tyuterev, V. G.; Adkins, E. M.; Baker, A.; Barber, A.; Canev, E.; Császár, A. G.; Egorov, O.; Fleisher, A. J.; Foltynowicz, A.; Furtenbacher, T.; Harrison, J. J.; Hartmann, J.; Horneman, V.; Huang, X.; Karman, T.; Karnsa, J.; Kassi, S.; Kleiner, I.; Kofman, V.; Kwabia-Tchana, F.; Lee, T. J.; Longo, D. A.; Lukashevskaya, A. A.; Lyulin, O. M.; Makhneva, V. Y.; Massie, S. T.; Melosso, M.; Mikhailenko, S. N.; Mondelain, D.; Müller, H. S. P.; Naumenko, O. V.; Perrin, A.; Polyansky, O. L.; Raddaoui, E.; Rastonah, P. L.; Reed, Z. D.; Rey, M.; Richard, C.; Tóbiás, R.; Sadieky, I.; Schwenke, D. W.; Starikova, E.; Sung, K.; Tamassia, F.; Tashkun, S. A.; Auwera, J. V.; Vigasina, A. A.; Villanueva, G. L.; Vispoel, B.; Wagner, G.; Yurchenko, S. N. The HITRAN 2020 molecular spectroscopic database. *J. Quant. Spectrosc. Rad. Transf.* **2022,** *276*, 107949.
5. McClatchey, R. A.; Benedict, W. S.; Clough, S. A.; Burch, D. E.; Calfee, R. F.; Fox, K.; Rothman, L. S.; Garing, J. S. AFCRL atmospheric absorption line parameters compilation. Technical report, Air Force Cambridge Research Laboratories, Hanscom Field, Bedford, 1973.

6. Endres, C. P.; Schlemmer, S.; Schilke, P.; Stutzki, J.; Müller, H. S. P. The Cologne database for molecular spectroscopy, CDMS, in the virtual atomic and molecular data centre, VAMDC. *J. Mol. Spectrosc.* **2016,** *327*, 95–104.
7. Tennyson, J.; Yurchenko, S. N.; Al-Refaie, A. F.; Barton, E. J.; Chubb, K. L.; Coles, P. A.; Diamantopoulou, S.; Gorman, M. N.; Hill, C.; Lam, A. Z.; Lodi, L.; McKemmish, L. K.; Na, Y.; Owens, A.; Polyansky, O. L.; Sousa-Silva, C.; Underwood, D. S.; Yachmenev, A.; Zak, E. The ExoMol database: molecular line lists for exoplanet and other hot atmospheres. *J. Mol. Spectrosc.* **2016,** *327*, 73–94.
8. Tennyson, J.; Yurchenko, S. N.; Zhang, J.; Bowesman, C. A.; Brady, R. P.; Buldyreva, J.; Chubb, K. L.; Gamache, R. R.; Gorman, M. N.; Guest, E. R.; Hill, C.; Kefala, K.; Lynas-Gray, A. E.; Mellor, T. M.; McKemmish, L. K.; Mitev, G. B.; Mizus, I. I.; Owens, A.; Peng, Z.; Perri, A. N.; Pezzella, M.; Polyansky, O. L.; Qu, Q.; Semenov, M.; Smola, O.; Solokov, A.; Somogyi, W.; Upadhyay, A.; Wright, S. O.; Zobov, N. F. The 2024 release of the ExoMol database: molecular line lists for exoplanet and other hot atmospheres. *J. Quant. Spectrosc. Rad. Transf.* **2024** (submitted).
9. Jacquinet-Husson, N.; Armante, R.; Scott, N. A.; Chedin, A.; Crepeau, L.; Boutammine, C.; Bouhdaoui, A.; Crevoisier, C.; Capelle, V.; Boonne, C.; Poulet-Crovisier, N.; Barbe, A.; Benner, D. C.; Boudon, V.; Brown, L. R.; Buldyreva, J.; Campargue, A.; Coudert, L. H.; Devi, V. M.; Down, M. J.; Drouin, B. J.; Fayt, A.; Fittschen, C.; Flaud, J. M.; Gamache, R. R.; Harrison, J. J.; Hill, C.; Hodnebrog, O.; Hu, S. M.; Jacquemart, D.; Jolly, A.; Jimenez, E.; Lavrentieva, N. N.; Liu, A. W.; Lodi, L.; Lyulin, O. M.; Massie, S. T.; Mikhailenko, S.; Mueller, H. S. P.; Naumenko, O. V.; Nikitin, A.; Nielsen, C. J.; Orphal, J.; Perevalov, V. I.; Perrin, A.; Polovtseva, E.; Predoi-Cross, A.; Rotger, M.; Ruth, A. A.; Yu, S. S.; Sung, K.; Tashkun, S. A.; Tennyson, J.; Tyuterev, V. I. G.; Auwera, J. V.; Voronin, B. A.; Makie, A. The 2015 edition of the GEISA spectroscopic database. *J. Mol. Spectrosc.* **2016,** *327*, 31–72.
10. Rothman, L. S. History of the hitran database. *Nat. Rev. Phys.* **2021,** *3*, 302–304.
11. Gordon, I. E.; Rothman, L. S.; Hill, C.; Kochanov, R. V.; Tan, Y.; Bernath, P. F.; Birk, M.; Boudon, V.; Campargue, A.; Chance, K. V.; Drouin, B. J.; Flaud, J.-M.; Gamache, R. R.; Hodges, J. T.; Jacquemart, D.; Perevalov, V. I.; Perrin, A.; Shine, K. P.; Smith, M.-A. H.; Tennyson, J.; Toon, G. C.; Tran, H.; Tyuterev, V. G.; Barbe, A.; Császár, A. G.; Devi, V. M.; Furtenbacher, T.; Harrison, J. J.; Hartmann, J.-M.; Jolly, A.; Johnson, T. J.; Karman, T.; Kleiner, I.; Kyuberis, A. A.; Loos, J.; Lyulin, O. M.; Massie, S. T.; Mikhailenko, S. N.; Moazzen-Ahmadi, N.; Müller, H. S. P.; Naumenko, O. V.; Nikitin, A. V.; Polyansky, O. L.; Rey, M.; Rotger, M.; Sharpe, S. W.; Sung, K.; Starikova, E.; Tashkun, S. A.; Auwera, J. V.; Wagner, G.; Wilzewski, J.; Wcisło, P.; Yu, S.; Zak, E. J. The HITRAN 2016 molecular spectroscopic database. *J. Quant. Spectrosc. Rad. Transf.* **2017,** *203*, 3–69.
12. Gamache, R. R.; Roller, C.; Lopes, E.; Gordon, I. E.; Rothman, L. S.; Polyansky, O. L.; Zobov, N. F.; Kyuberis, A. A.; Tennyson, J.; Yurchenko, S. N.; Császár, A. G.; Furtenbacher, T.; Huang, X.; Schwenke, D. W.; Lee, T. J.; Drouin, B. J.; Tashkun, S. A.; Perevalov, V. I.; Kochanov, R. V. Total internal partition sums for 166 isotopologues of 51 molecules important in planetary atmospheres: Application to HITRAN 2016 and beyond. *J. Quant. Spectrosc. Rad. Transf.* **2017,** *203*, 70–87.
13. https://spec.jpl.nasa.gov/ftp/pub/catalog/archive/c018005.egy. JPL website, last accessed on February 13, 2025.
14. Kukolich, S. G. Measurement of the molecular g values in H_2O and D_2O and hyperfine structure in H_2O. *J. Chem. Phys.* **1969,** *50*, 3751–3755.
15. Cazzoli, G.; Puzzarini, C.; Harding, M. E.; Gauss, J. The hyperfine structure in the rotational spectrum of water: Lamb-dip technique and quantum-chemical calculations. *Chem. Phys. Lett.* **2009,** *473*, 21–25.

16. Watson, J. K. G. Simplification of the molecular vibration-rotation Hamiltonian. *Mol. Phys.* **1968,** *15*, 479–490.
17. Furtenbacher, T.; Coles, P. A.; Tennyson, J., et al. Empirical Rovibrational Energy Levels of Ammonia up to 7500 Cm^{-1}. *J. Quant. Spectrosc. Rad. Transf.* **2020,** *251*, 107027.
18. Ritz, W. On a new law of series spectra. *Astrophys. J.* **1908,** *28*, 237–243.
19. Császár, A. G.; Czakó, G.; Furtenbacher, T.; Mátyus, E. An active database approach to complete spectra of small molecules. *Annu. Rep. Comput. Chem.* **2007,** *3*, 155–176.
20. Furtenbacher, T.; Császár, A. G.; Tennyson, J. MARVEL: measured active rotational-vibrational energy levels. *J. Mol. Spectrosc.* **2007,** *245*, 115–125.
21. Furtenbacher, T.; Császár, A. G. MARVEL: measured active rotational-vibrational energy levels. II. Algorithmic improvements. *J. Quant. Spectrosc. Rad. Transf.* **2012,** *113*, 929–935.
22. Tóbiás, R.; Furtenbacher, T.; Tennyson, J.; Császár, A. G. Accurate empirical rovibrational energies and transitions of $H_2{}^{16}O$. *Phys. Chem. Chem. Phys.* **2019,** *21*, 3473–3495.
23. Furtenbacher, T.; Tóbiás, R.; Tennyson, J., et al. The W2024 Database of the Water Isotopologue $H_2{}^{16}O$. *Sci. Data.* **2024,** *11*, 1058.
24. Furtenbacher, T.; Szabó, I.; Császár, A. G.; Bernath, P. F.; Yurchenko, S. N.; Tennyson, J. Experimental energy levels and partition function of the $^{12}C_2$ molecule. *Astrophys. J. Suppl. S.* **2016,** *224*, 44.
25. McKemmish, L. K.; Syme, A.-M.; Borsovszky, J.; Yurchenko, S. N.; Tennyson, J.; Furtenbacher, T.; Császár, A. G. An update to the MARVEL data set and ExoMol line list for $^{12}C_2$. *Mon. Not. R. Astron. Soc.* **2020,** *497*, 1081–1097.
26. Furtenbacher, T.; Hegedus, S. T.; Tennyson, J., et al. Analysis of Measured High-Resolution Doublet Rovibronic Spectra and Related Line Lists of ^{12}CH and ^{16}OH. *Phys. Chem. Chem. Phys.* **2022,** *24*, 19287–19301.
27. Darby-Lewis, D.; Shah, H.; Joshi, D.; Khan, F.; Kauwo, M.; Sethi, N.; Bernath, P. F.; Furtenbacher, T.; Tóbiás, R.; Császár, A. G.; Tennyson, J. MARVEL analysis of the measured high-resolution spectra of ^{14}NH. *J. Mol. Spectrosc.* **2019,** *362*, 69–76.
28. Furtenbacher, T.; Horváth, M.; Koller, D.; Sólyom, P.; Balogh, A.; Balogh, I.; Császár, A. G. MARVEL analysis of the measured high-resolution rovibronic spectra and definitive ideal-gas thermochemistry of the $^{16}O_2$ molecule. *J. Phys. Chem. Ref. Data* **2019,** *48*, 023101.
29. McKemmish, L. K.; Masseron, T.; Sheppard, S.; Sandeman, E.; Schofield, Z.; Furtenbacher, T.; Császár, A. G.; Tennyson, J.; Sousa-Silva, C. MARVEL analysis of the measured high-resolution rovibronic spectra of $^{48}Ti\,^{16}O$. *Astrophys. J. Suppl. S* **2017,** *228*, 15.
30. McKemmish, L. K.; Borsovszky, J.; Goodhew, K. L.; Sheppard, S.; Bennett, A. F. V.; Martin, A. D. J.; Singh, A.; Sturgeon, C. A. J.; Furtenbacher, T.; Császár, A. G.; Tennyson, J. MARVEL analysis of the measured high-resolution rovibronic spectra of $^{90}Zr\,^{16}O$. *Astrophys. J.* **2018,** *867*, 33.
31. Ibrahim, M. T. I.; Alatoom, D.; Furtenbacher, T., et al. MARVEL Analysis of High-Resolution Rovibrational Spectra of $^{13}C^{16}O_2$. *J. Comp. Chem.* **2024,** *45*, 969–984.
32. Alatoom, D.; Ibrahim, M. T. I.; Furtenbacher, T., et al. MARVEL Analysis of High-Resolution Rovibrational Spectra of $^{16}O^{12}C^{18}O$. *J. Comp. Chem.* **2024**.
33. Furtenbacher, T.; Szidarovszky, T.; Mátyus, E.; Fábri, C.; Császár, A. G. Analysis of the rotational-vibrational states of the molecular ion H_3^+. *J. Chem. Theor. Comput.* **2013,** *9*, 5471–5478.
34. Furtenbacher, T.; Szidarovszky, T.; Fábri, C.; Császár, A. G. MARVEL analysis of the rotational-vibrational states of the molecular Ions H_2D^+ and D_2H^+. *Phys. Chem. Chem. Phys.* **2013,** *15*, 10181–10193.

35. Furtenbacher, T.; Császár, A. G. On Employing $H_2{}^{16}O$, $H_2{}^{17}O$, $H_2{}^{18}O$, and $D_2{}^{16}O$ Lines as Frequency Standards in the 15−170 cm^{-1} Window. *J. Quant. Spectrosc. Rad. Transf.* **2008,** *109*, 1234–1251.
36. Tennyson, J.; Bernath, P. F.; Brown, L. R.; Campargue, A.; Carleer, M. R.; Császár, A. G.; Gamache, R. R.; Hodges, J. T.; Jenouvrier, A.; Naumenko, O. V.; Polyansky, O. L.; Rothman, L. S.; Toth, R. A.; Vandaele, A. C.; Zobov, N. F.; Daumont, L.; Fazliev, A. Z.; Furtenbacher, T.; Gordon, I. E.; Mikhailenko, S. N.; Shirin, S. V. IUPAC critical evaluation of the rotational-vibrational spectra of water vapor. Part I. Energy levels and transition wavenumbers for $H_2{}^{17}O$ and $H_2{}^{18}O$. *J. Quant. Spectrosc. Rad. Transf.* **2009,** *110*, 573–596.
37. Tennyson, J.; Bernath, P. F.; Brown, L. R.; Campargue, A.; Császár, A. G.; Daumont, L.; Gamache, R. R.; Hodges, J. T.; Naumenko, O. V.; Polyansky, O. L.; Rothman, L. S.; Toth, R. A.; Vandaele, A. C.; Zobov, N. F.; Fally, S.; Fazliev, A. Z.; Furtenbacher, T.; Gordon, I. E.; Hu, S.-M.; Mikhailenko, S. N.; Voronin, B. A. IUPAC critical evaluation of the rotational-vibrational spectra of water vapor. Part II. Energy levels and transition wavenumbers for $HD^{16}O$, $HD^{17}O$, and $HD^{18}O$. *J. Quant. Spectrosc. Rad. Transf.* **2010,** *111*, 2160–2184.
38. Tennyson, J.; Bernath, P. F.; Brown, L. R., et al. IUPAC Critical Evaluation of the Rotational-Vibrational Spectra of Water Vapor. Part III. Energy Levels and Transition Wavenumbers for $H_2{}^{16}O$. *J. Quant. Spectrosc. Rad. Transf.* **2013,** *117*, 29–80.
39. Tennyson, J.; Bernath, P. F.; Brown, L. R., et al. IUPAC Critical Evaluation of the Rotational-Vibrational Spectra of Water Vapor. Part IV. Energy Levels and Transition Wavenumbers for $D_2{}^{16}O$, $D_2{}^{17}O$, and $D_2{}^{18}O$. *J. Quant. Spectrosc. Rad. Transf.* **2014,** *142*, 93–108.
40. Furtenbacher, T.; Tóbiás, R.; Tennyson, J., et al. W2020: A Database of Validated Rovibrational Experimental Transitions and Empirical Energy Levels of $H_2{}^{16}O$. *J. Phys. Chem. Ref. Data* **2020,** *49*, 033101.
41. Tóbiás, R.; Furtenbacher, T.; Simkó, I.; Császár, A. G.; Diouf, M. L.; Cozijn, F. M. J.; Staa, J. M. A.; Salumbides, E. J.; Ubachs, W. Spectroscopic-network-assisted precision spectroscopy and its application to water. *Nat. Commun.* **2020,** *11*, 1708.
42. Furtenbacher, T.; Tóbiás, R.; Tennyson, J., et al. The W2020 Database of Validated Rovibrational Experimental Transitions and Empirical Energy Levels of Water Isotopologues. Part II. $H_2{}^{17}O$ and $H_2{}^{18}O$ with an Update to $H_2{}^{16}O$. *J. Phys. Chem. Ref. Data* **2020,** *49*, 043103.
43. Rácsai, B.; Furtenbacher, T.; Fusina, L.; DiLonardo, G.; Császár, A. G. MARVEL analysis of the high-resolution rovibrational spectra of $H^{16}O^{35}Cl$. *J. Mol. Spectrosc.* **2022,** *384*, 111561.
44. Ecseri, G.; Simkó, I.; Furtenbacher, T.; Rácsai, B.; Fusina, L.; DiLonardo, G.; Peterson, K. A.; Császár, A. G. Joint survey of the experimental high-resolution spectra of $H^{16}O^{37}Cl$ and $H^{16}O^{35}Cl$ with a reanalysis of the $2\nu_2$ band. *J. Mol. Spectrosc.* **2023,** *397*, 111834.
45. Chubb, K. L.; Naumenko, O.; Keely, S., et al. MARVEL Analysis of the Measured High-Resolution Rovibrational Spectra of $H_2{}^{32}S$. *J. Quant. Spectrosc. Rad. Transf.* **2018,** *218*, 178–186.
46. Tennyson, J.; Furtenbacher, T.; Yurchenko, S. N.; Császár, A. G. Empirical rovibrational energy levels for nitrous oxide. *J. Quant. Spectrosc. Rad. Transf.* **2024,** *316*, 108902.
47. Tóbiás, R.; Furtenbacher, T.; Császár, A. G.; Naumenko, O. V.; Tennyson, J.; Flaud, J.-M.; Kumar, P.; Poirier, B. Critical evaluation of measured rotational-vibrational transitions of four sulphur isotopologues of $S^{16}O_2$. *J. Quant. Spectrosc. Rad. Transf.* **2018,** *208*, 152–163.
48. Chubb, K. L.; Joseph, M.; Franklin, J.; Choudhury, N.; Furtenbacher, T.; Császár, A. G.; Gaspard, G.; Oguoko, P.; Kelly, A.; Yurchenko, S. N.; Tennyson, J.; Sousa-Silva,

C. MARVEL analysis of the measured high-resolution spectra of C_2H_2. *J. Quant. Spectrosc. Rad. Transf.* **2018,** *204*, 42–55.
49. Al-Derzi, A. R.; Tennyson, J.; Yurchenko, S. N., et al. An Improved Rovibrational Linelist of Formaldehyde, $H_2{}^{12}C^{16}O$. *J. Quant. Spectrosc. Rad. Transf.* **2021,** *266*, 107563.
50. AlDerzi, A. R.; Furtenbacher, T.; Yurchenko, S. N.; Tennyson, J.; Császár, A. G. MARVEL analysis of the measured high-resolution spectra of $^{14}NH_3$. *J. Quant. Spectrosc. Rad. Transf.* **2015,** *161*, 117–130.
51. Fábri, C.; Mátyus, E.; Furtenbacher, T.; Nemes, L.; Mihály, B.; Zoltáni, T.; Császár, A. G. Variational quantum mechanical and active database approaches to the rotational-vibrational spectroscopy of ketene, H_2CCO. *J. Chem. Phys.* **2011,** *135*, 094307.
52. Furtenbacher, T.; Árendás, P.; Mellau, G.; Császár, A. G. Simple molecules as complex systems. *Sci. Rep.* **2014,** *4*, 4654.
53. Árendás, P.; Furtenbacher, T.; Császár, A. G. On spectra of spectra. *J. Math. Chem.* **2016,** *54*, 806–822.
54. Császár, A. G.; Furtenbacher, T.; Árendás, P. Small molecules – big data. *J. Phys. Chem. A* **2016,** *120*, 8949–8969.
55. Császár, A. G.; Furtenbacher, T. Spectroscopic networks. *J. Mol. Spectrosc.* **2011,** *266*, 99–103.
56. Császár, A. G.; Fábri, C.; Szidarovszky, T.; Mátyus, E.; Furtenbacher, T.; Czakó, G. The fourth age of quantum chemistry: molecules in motion. *Phys. Chem. Chem. Phys.* **2012,** *14*, 1085–1106.
57. Császár, A. G.; Tarczay, G.; Leininger, M. L.; Polyansky, O. L.; Tennyson, J.; Allen, W. D. Dream or reality: complete basis set full configuration interaction potential energy hypersurfaces. In *Spectroscopy from Space;* Demaison, J., Sarka, K., Cohen, E. A., Eds.; Kluwer: Dordrecht, 2001; pp. 317–339.
58. Diouf, M. L.; Tóbiás, R.; Simkó, I., et al. Network-Based Design of near-Infrared Lamb-Dip Experiments and the Determination of Pure Rotational Energies of $H_2{}^{18}O$ at kHz Accuracy. *J. Phys. Chem. Ref. Data* **2021,** *50*, 023106.
59. Mellau, G. C.; Makhnev, V. Y.; Gordon, I. E.; Zobov, N. F. An experimentally-accurate and complete room-temperature infrared HCN line-list for the HITRAN database. *J. Quant. Spectrosc. Rad. Transf.* **2021,** *270*, 107666.
60. Furtenbacher, T., Tóbiás, R.; Tennyson, J.; Gamache, R.R.; Császár, A.G. Repository for the W2024 database of the water isotopologue $H_2{}^{16}O$. https://doi.org/10.17605/OSF.IO/4E237
61. Maksyutenko, P.; Rizzo, T. R.; Boyarkin, O. V. A direct measurement of the dissociation energy of water. *J. Chem. Phys.* **2006,** *125*, 181101.
62. Grechko, M.; Boyarkin, O. V.; Rizzo, T. R.; Maksyutenko, P.; Zobov, N. F.; Shirin, S.; Lodi, L.; Tennyson, J.; Császár, A. G.; Polyansky, O. L. State-selective spectroscopy of water up to its first dissociation limit. *J. Chem. Phys.* **2009,** *131*, 221105.
63. Partridge, H.; Schwenke, D. W. The determination of an accurate isotope dependent potential energy surface for water from extensive *ab initio* calculations and experimental data. *J. Chem. Phys.* **1997,** *106*, 4618–4639.
64. Schwenke, D. W. First principles prediction of isotopic shifts in H_2O. *J. Chem. Phys.* **2003,** *118*, 6898–6904.
65. Huang, X.; Schwenke, D. W.; Lee, T. J. An accurate global potential energy surface, dipole moment surface, and rovibrational frequencies for NH_3. *J. Chem. Phys.* **2008,** *129*, 214304.
66. Rey, M.; Nikitin, A. V.; Babikov, Y. L.; Tyuterev, V. G. TheoReTS – an information system for theoretical spectra based on variational predictions from molecular potential energy and dipole moment surfaces. *J. Mol. Spectrosc.* **2016,** *327*, 138–158.

67. Kassi, S.; Macko, P.; Naumenko, O., et al. The Absorption Spectrum of Water near 750 Nm by CW-CRDS: Contribution to the Search of Water Dimer Absorption. *Phys. Chem. Chem. Phys.* **2005,** *7*, 2460–2467.
68. Polyansky, O. L.; Zobov, N. F.; Viti, S.; Tennyson, J.; Bernath, P. F.; Wallace, L. High temperature rotational transitions of water in sunspot and laboratory spectra. *J. Mol. Spectrosc.* **1997,** *186*, 422–447.
69. Esplin, M. P.; Huppi, R. J.; Sakai, H.; Vanasse, G. A.; Rothman, L. S. Absorption measurements of CO_2 and H_2O at high resolution and elevated temperatures. Tech. Rep. AFGL-TR-82-0057 (Utah State University).
70. Hänsch, T. W. Nobel lecture: passion for precision. *Rev. Mod. Phys.* **2006,** *78*, 1297–1309.
71. Kandula, D. Z.; Gohle, C.; Pinkert, T. J.; Ubachs, W.; Eikema, S. E. Extreme ultraviolet frequency comb metrology. *Phys. Rev. Lett.* **2010,** *105*, 063001.
72. Newman, M. E. J. *Networks*. Oxford University Press: Oxford, 2010.
73. Matsushima, F.; Odashima, H.; Iwasaki, T.; Tsunekawa, S.; Takagi, K. Frequency measurement of pure rotational transitions of H_2O from 0.5 to 5 THz. *J. Mol. Spectrosc.* **1995,** *352*, 371–378.
74. de Natale, P.; Lorini, L.; Inguscio, M., et al. Accurate Frequency Measurement for H_2O and $^{16}O_3$ in the 119 cm^{-1} OH Atmospheric Window. *Appl. Optics* **1997,** *36*, 8526–8532.
75. Horneman, V.-M.; Anttila, R.; Alanko, S.; Pietilä, J. Transferring calibration from CO_2 laser lines to far infrared water lines with the aid of the ν_2 band of OCS and the ν_2, $\nu_1 - \nu_2$, and $\nu_1 + \nu_2$ bands of $^{13}CS_2$: Molecular constants of $^{13}CS_2$. *J. Mol. Spectrosc.* **2005,** *234*, 238–254.
76. Toureille, M.; Koroleva, A. O.; Mikhailenko, S. N., et al. Water Vapor Absorption Spectroscopy and Validation Tests of Databases in the Far-Infrared (50–720 cm^{-1}). Part 1: Natural Water. *J. Quant. Spectrosc. Rad. Transf.* **2022,** *291*, 108326.
77. Mikhailenko, S. N.; Karlovets, E. V.; Koroleva, A. O., et al. The Far Infrared Absorption Spectrum of $D_2{}^{16}O$, $D_2{}^{17}O$, and $D_2{}^{18}O$: Experimental Line Positions, Empirical Energy Levels and Recommended Line Lists. *J. Phys. Chem. Ref. Data* **2024,** *53*.
78. Albritton, D. L.; Harrop, W. J.; Schmeltekopf, A. L.; Zare, R. N.; Crow, E. L. A critique of the term value approach to determining molecular constants from the spectra of diatomic molecules. *J. Mol. Spectrosc.* **1973,** *46*, 67–88.
79. Aslund, N. A numerical method for the simultaneous determination of term values and molecular constants. *J. Mol. Spectrosc.* **1974,** *50*, 424–434.
80. Pliva, J.; Telfair, W. B. Correlations and accuracy of estimation of spectroscopic constants and term values. *J. Mol. Spectrosc.* **1974,** *53*, 221–245.
81. Flaud, J.-M.; Camy-Peyret, C.; Maillard, J. P. Higher ro-vibrational levels of H_2O deduced from high resolution oxygen-hydrogen flame spectra between 2800–6200 cm^{-1}. *Mol. Phys.* **1976,** *32*, 499–521.
82. Lindsay, C. M.; McCall, B. J. Comprehensive evaluation and compilation of H_3^+ spectroscopy. *J. Mol. Spectrosc.* **2001,** *210*, 60–83.
83. Tashkun, S. A.; Perevalov, V. I.; Teffo, J.-L.; Bykov, A. D.; Lavrentieva, N. N. CDSD-1000, the high-temperature carbon dioxide spectroscopic databank. *J. Quant. Spectrosc. Rad. Transf.* **2003,** *82*, 165–196.
84. Tóbiás, R.; Bérczi, K.; Szabó, C.; Császár, A. G. autoECART: automatic energy conservation analysis of rovibronic transitions. *J. Quant. Spectrosc. Rad. Transf.* **2021,** *272*, 107756.
85. Árendás, P.; Furtenbacher, T.; Császár, A. G. From bridges to cycles in spectroscopic networks. *Sci. Rep.* **2020,** *10*, 1–13.
86. Árendás, P.; Furtenbacher, T.; Császár, A. G. Selecting lines for spectroscopic (re) measurements to improve the accuracy of absolute energies of rovibronic quantum states. *J. Cheminform* **2021,** *13*, 67.

87. Árendás, P.; Furtenbacher, T.; Császár, A. G. Spectroscopic heat maps reveal how to design experiments to improve the uncertainties of transitions and energy levels present in line-by-line databases. *J. Quant. Spectrosc. Rad. Transf.* **2024,** *315*, 108878.
88. Diouf, M. L.; Tóbiás, R.; Cozijn, F. M. J.; Salumbides, E. J.; Fábri, C.; Puzzarini, C.; Császár, A. G.; Ubachs, W. Parity-pair-mixing effects in nonlinear spectroscopy of HDO. *Opt. Express* **2022,** *30*, 46040–46059.
89. Diouf, M. L.; Tóbiás, R.; van der Schaaf, T. S., et al. Ultraprecise Relative Energies in the (2 0 0) Vibrational Band of $H_2{}^{16}O$. *Mol. Phys.* **2022,** *120*, e2050430.
90. Castrillo, A.; Fasci, E.; Furtenbacher, T.; D'Agostino, V.; Khan, M. A.; Gravina, S.; Gianfrani, L.; Császár, A. G. On the $^{12}C_2H_2$ near-infrared spectrum: absolute transition frequencies and an improved spectroscopic network at the kHz accuracy level. *Phys. Chem. Chem. Phys.* **2023,** *25*, 23614–23625.
91. Tóbiás, R.; Diouf, M. L.; Cozijn, F. M., et al. All Paths Lead to Hubs in the Spectroscopic Networks of Water Isotopologues $H_2{}^{16}O$ and $H_2{}^{18}O$. *Commun. Chem.* **2024,** 7, 34.
92. Ubachs, W.; Császár, A. G.; Diouf, M. L.; Cozijn, F. M.; Tóbiás, R. A network approach for the accurate characterization of water lines observable in astronomical masers and extragalactic environments. *ACS Earth Space Chem.* **2024,** *8*, 1901–1912.
93. Coles, P. A.; Yurchenko, S. N.; Tennyson, J. ExoMol Molecular Line Lists – XXXV. A Rotation-Vibration Line List for Hot Ammonia. *Mon. Not. R. Astron. Soc.* **2019,** *490*, 4638–4647.
94. Kleiner, I.; Fraser, G. T.; Hougen, J. T.; Pine, A. S. Molecular-beam optothermal spectrum of the OH stretching band of methanol. *J. Mol. Spectrosc.* **1991,** *147*, 155–172.
95. Kleiner, I. Asymmetric-top molecules containing one methyl-like internal rotor: Methods and codes for fitting and predicting spectra. *J. Mol. Spectrosc.* **2010,** *260*, 1–18.
96. Costain, C. C. An empirical formula for the microwave spectrum of ammonia. *Phys. Rev.* **1951,** *82*, 108.
97. Sasada, H.; Endo, Y.; Hirota, E.; Poynter, R.; Margolis, J. Microwave and Fourier-transform infrared spectroscopy of the $\nu_4 = 1$ and $\nu_2 = 2\,s$ states of NH_3. *J. Mol. Spectrosc.* **1992,** *151*, 33–53.
98. Kleiner, I.; Tarrago, G.; Brown, L. R. Positions and Intensities in the $3\nu_2/\nu_2 + \nu_4$ Vibrational System of $^{14}NH_3$ near 4 μm. *J. Mol. Spectrosc.* **1995,** *173*, 120–145.
99. Cottaz, C.; Kleiner, I.; Tarrago, G., et al. Line Positions and Intensities in the $2\nu_2/\nu_4$ Vibrational System of $^{14}NH_3$ near 5–7 μm. *J. Mol. Spectrosc.* **2000,** *203*, 285–309.
100. Cottaz, C.; Tarrago, G.; Kleiner, I.; Brown, L. R. Assignments and intensities of $^{14}NH_3$ hot bands in the 5- to 8-μm ($3\nu_2 - \nu_2$, $\nu_2 + \nu_4 - \nu_2$) and 4-μm ($4\nu_2 - \nu_2$, $\nu_1 - \nu_2$, $\nu_3 - \nu_2$ and $2\nu_4 - \nu_2$) regions. *J. Mol. Spectrosc.* **2001,** *209*, 30–49.
101. Sung, K.; Brown, L. R.; Huang, X., et al. Extended Line Positions, Intensities, Empirical Lower State Energies and Quantum Assignments of NH_3 from 6300 to 7000 cm^{-1}. *J. Quant. Spectrosc. Rad. Transf.* **2012,** *113*, 1066–1083.
102. Chen, P.; Pearson, J. C.; Pickett, H. M.; Matsuura, S.; Blake, G. A. Measurements of $^{14}NH_3$ in the $\nu_2 = 1$ state by a solid-state, photomixing, THz spectrometer, and a simultaneous analysis of the microwave, terahertz, and infrared transitions between the ground and ν_2 inversion-rotation levels. *J. Mol. Spectrosc.* **2006,** *236* (1), 116–126.
103. Yu, S.; Pearson, J. C.; Drouin, B. J.; Sung, K.; Pirali, O.; Vervloet, M.; Martin-Drumel, M.-A.; Endres, C. P.; Shiraishi, T.; Kobayashi, K.; Matsushima, F. Submillimeter-wave and far-infrared spectroscopy of high-J transitions of the ground and $\nu_2 = 1$ states of ammonia. *J. Chem. Phys.* **2010,** *133*.
104. Pearson, J. C.; Yu, S.; Pirali, O. Modeling the spectrum of the $2\nu_2$ and ν_4 states of ammonia to experimental accuracy. *J. Chem. Phys.* **2016,** *145*.
105. Pearson, J.; Yu, S.; Pearson, J.; Sung, K.; Drouin, B.; Pirali, O. Extended measurements and an experimental accuracy effective Hamiltonian model for the $3\nu_2$ and $\nu_4 + \nu_2$ states of ammonia. *J. Mol. Spectrosc.* **2018,** *353*, 60–66.

106. Wei, H.; Carrington, T., Jr. The discrete variable representation of a triatomic Hamiltonian in bond length-bond angle coordinates. *J. Chem. Phys.* **1992,** *97*, 3029–3037.
107. Bramley, M. J.; Carrington, T., Jr. A general discrete variable method to calculate vibrational energy levels of three- and four-atom molecules. *J. Chem. Phys.* **1993,** *99*, 8519–8541.
108. Szalay, V. Discrete variable representations of differential operators. *J. Chem. Phys.* **1993,** *99*, 1978–1984.
109. Tennyson, J.; Henderson, J. R.; Fulton, N. G. DVR3D for the fully pointwise calculation of ro-vibrational spectra of triatomic-molecules. *Comput. Phys. Commun.* **1995,** *86*, 175–198.
110. Light, J. C.; Carrington, T. Discrete variable representations and their utilization. *Adv. Chem. Phys.* **2000,** *114*, 263–310.
111. Mladenovic, M. Discrete variable approaches to tetratomic molecules-Part I: DVR(6) and DVR(3)+ DGB methods. *Spectrochim. Acta A* **2002,** *58A*, 795–807.
112. Szalay, V.; Czakó, G.; Nagy, A.; Furtenbacher, T.; Császár, A. G. On one-dimensional discrete variable representations with general basis functions. *J. Chem. Phys.* **2003,** *119*, 10512–10518.
113. Tennyson, J.; Kostin, M. A.; Barletta, P.; Harris, G. J.; Polyansky, O. L.; Ramanlal, J.; Zobov, N. F. DVR3D: a program suite for the calculation of rotation-vibration spectra of triatomic molecules. *Comput. Phys. Commun.* **2004,** *163*, 85–116.
114. Mátyus, E.; Czakó, G.; Sutcliffe, B. T.; Császár, A. G. Vibrational energy levels with arbitrary potentials using the Eckart-Watson Hamiltonians and the discrete variable representation. *J. Chem. Phys.* **2007,** *127*, 084102.
115. Bowman, J. M.; Carrington, T.; Meyer, H.-D. Variational quantum approaches for computing vibrational energies of polyatomic molecules. *Mol. Phys.* **2008,** *106*, 2145–2182.
116. Mátyus, E.; Czakó, G.; Császár, A. G. Toward black-box-type full- and reduced-dimensional variational (ro)vibrational computations. *J. Chem. Phys.* **2009,** *130*, 134112.
117. Fábri, C.; Mátyus, E.; Császár, A. G. Rotating full- and reduced-dimensional quantum chemical models of molecules. *J. Chem. Phys.* **2011,** *134*, 074105.
118. Szalay, V.; Szidarovszky, T.; Czakó, G.; Császár, A. G. A paradox of grid-based representation techniques: accurate eigenvalues from inaccurate matrix elements. *J. Math. Chem.* **2012,** *50*, 636–651.
119. Wilson, E. B., Jr; Decius, J. C.; Cross, P. C. *Molecular Vibrations: The Theory of Infrared and Raman Vibrational Spectra;* McGraw Hill: New York, 1955.
120. Kroto, H. W. *Molecular Rotation Spectra;* Dover: New York, 1992.
121. Nielsen, H. H. The vibration-rotation energies of molecules. *Rev. Mod. Phys.* **1951,** *23*, 90–136.
122. Clabo, D. A.; Allen, W. D.; Remington, R. B.; Yamaguchi, Y.; Schaefer, H. F., III A systematic study of molecular vibrational anharmonicity and vibration-rotation interaction by self-consistent-field higher derivative methods. asymmetric top molecules. *Chem. Phys.* **1988,** *123*, 187–239.
123. Allen, W. D.; Yamaguchi, Y.; Császár, A. G.; Clabo, D. A., Jr; Remington, R. B.; Schaefer, H. F., III A systematic study of molecular vibrational anharmonicity and vibration-rotation interaction by self-consistent-field higher derivative methods. Linear polyatomic molecules. *Chem. Phys.* **1990,** *145*, 427–466.
124. Born, M.; Oppenheimer, J. R. Zur quantentheorie der molekeln. *Ann. Phys. (Berlin)* **1927,** *84*, 457–484.
125. Tennyson, J. Accurate variational calculations for line lists to model the vibration-rotation spectra of hot astrophysical atmospheres. *WIREs Comp. Mol. Sci.* **2011,** *2*, 698–715.

126. Pavanello, M.; Adamowicz, L.; Alijah, A.; Zobov, N. F.; Mizus, I. I.; Polyansky, O. L.; Tennyson, J.; Szidarovszky, T.; Császár, A. G.; Berg, M.; Petrignani, A.; Wolf, A. Precision measurements and computations of transition energies in rotationally cold triatomic hydrogen ions up to the mid-visible spectral range. *Phys. Rev. Lett.* **2012,** *108*, 023002.
127. Bucknell, M. G.; Handy, N. C. Vibration-rotation wavefunctions and energies for the ground electronic state of the water molecule by a variational method. *Mol. Phys.* **1974,** *28*, 777–792.
128. Whitehead, R. J.; Handy, N. C. Variational calculation of vibration-rotation energy levels for triatomic molecules. *J. Mol. Spectrosc.* **1975,** *55*, 356–373.
129. Carter, S.; Handy, N. C. The variational method for the calculation of ro-vibrational energy levels. *Comput. Phys. Rep.* **1986,** *5*, 117–171.
130. Handy, N. C. The calculation of vibrational energy levels by semiclassical and quantum methodology: a review. *Int. Rev. Phys. Chem.* **1989,** *8*, 275–288.
131. Poulin, N. M.; Bramley, M. J.; Carrington, T., Jr.; Kjaergaard, H. G.; Henry, B. R. Calculation of vibrational ($J = 0$) excitation energies and band intensities of formaldehyde using the recursive residue generation method. *J. Chem. Phys.* **1996,** *104*, 7807–7820.
132. Carter, S.; Bowman, J. M.; Handy, N. C. Extensions and tests of MULTIMODE: a code to obtain accurate vibration/rotation energies of many-mode molecules. *Theor. Chem. Acc.* **1998,** *100*, 191–198.
133. Yurchenko, S. N.; Thiel, W.; Jensen, P. Theoretical rovibrational energies (TROVE): a robust numerical approach to the calculation of rovibrational energies for polyatomic molecules. *J. Mol. Spectrosc.* **2007,** *245*, 126–140.
134. Wang, X.-G.; Carrington, T. Computing rovibrational levels of methane with curvilinear internal vibrational coordinates and an Eckart frame. *J. Chem. Phys.* **2013,** *138*, 104106.
135. Manzhos, S.; Carrington, T., Jr Using an internal coordinate Gaussian basis and a space-fixed Cartesian coordinate kinetic energy operator to compute a vibrational spectrum with rectangular collocation. *J. Chem. Phys.* **2016,** *145*, 224110.
136. Fábri, C.; Quack, M.; Császár, A. G. On the use of nonrigid-molecular symmetry in nuclear-motion computations employing a discrete variable representation: a case study of the bending energy levels of CH_5^+. *J. Chem. Phys.* **2017,** *147*, 134101.
137. Louck, J. D.; Galbraith, H. W. Eckart vectors, Eckart frames, and polyatomic molecules. *Rev. Mod. Phys.* **1976,** *48*, 69–106.
138. Fábri, C.; Mátyus, E.; Császár, A. G. Numerically constructed internal-coordinate Hamiltonian with Eckart embedding and its application for the inversion tunneling of ammonia. *Spectrochim. Acta A* **2014,** *119*, 84–89.
139. Bunker, P. R.; Jensen, P. *Molecular Symmetry and Spectroscopy;* NRC Research Press: Ottawa, 2006.
140. Császár, A. G.; Fábri, C.; Sarka, J. Quasistructural molecules. *WIREs Comp. Mol. Sci.* **2019,** *10*.
141. Lanczos, C. An iteration method for the solution of the eigenvalue problem of linear differential and integral operators. *J. Res. Natl. Bur. Stand.* **1950,** *45*, 255–282.
142. Fábri, C.; Sarka, J.; Császár, A. G. Communication: rigidity of the molecular ion H_5^+. *J. Chem. Phys.* **2014,** *140*, 051101.
143. Sarka, J.; Fábri, C.; Szidarovszky, T.; Császár, A. G.; Lin, Z.; McCoy, A. B. Modelling rotations, vibrations, and rovibrational couplings in astructural molecules – a case study based on the H_5^+ molecular ion. *Mol. Phys.* **2015,** *113*, 1873–1883.
144. Simkó, I.; Schran, C.; Brieuc, F.; Fábri, C.; Asvany, O.; Schlemmer, S.; Marx, D.; Császár, A. G. Quantum nuclear delocalization and its rovibrational fingerprints. *Angew. Chem. Int. Ed.* **2023,** *62* ISSN 1521-3773.

145. Császár, A. G.; Mátyus, E.; Szidarovszky, T.; Lodi, L.; Zobov, N. F.; Shirin, S. V.; Polyansky, O. L.; Tennyson, J. First-principles prediction and partial characterization of the vibrational states of water up to dissociation. *J. Quant. Spectrosc. Rad. Transf.* **2010,** *111*, 1043–1064.
146. Szidarovszky, T.; Császár, A. G.; Czakó, G. On the efficiency of treating singularities in triatomic variational vibrational computations. The vibrational states of H_3^+ up to dissociation. *Phys. Chem. Chem. Phys.* **2010,** *12*, 8373–8386.
147. Császár, A. G.; Simkó, I.; Szidarovszky, T., et al. Rotational-Vibrational Resonance States. *Phys. Chem. Chem. Phys.* **2020,** *22*, 15081–15104.
148. Mátyus, E.; Fábri, C.; Szidarovszky, T.; Czakó, G.; Allen, W. D.; Császár, A. G. Assigning quantum labels to variationally computed rotational-vibrational eigenstates of polyatomic molecules. *J. Chem. Phys.* **2010,** *133*, 034113.
149. Polyansky, O. L.; Kyuberis, A. A.; Zobov, N. F.; Tennyson, J.; Yurchenko, S. N.; Lodi, L. ExoMol molecular line lists XXX: a complete high-accuracy line list for water. *Mon. Not. R. Astron. Soc.* **2018,** *480*, 2597–2608.
150. Kassi, S.; Stoltmann, T.; Casado, M., et al. Lamb Dip CRDS of Highly Saturated Transitions of Water near 1.4 μm. *J. Chem. Phys.* **2018,** *148*, 054201.
151. Bonhoeffer, K. F.; Harteck, P. Über para- und orthowasserstoff. *Z. Phys. Chem.* **1929,** *4B*, 113–141.
152. Behler, J. First principles neural network potentials for reactive simulations of large molecular and condensed systems. *Angew. Chem. Int. Ed.* **2017,** *56*, 12828–12840.
153. Brett, C. M. A.; Frey, J. G.; Hinde, R.; Kuroda, Y.; Marquardt, R.; Pavese, F.; Quack, M.; Stohner, J.; Thor, A. J. *Quantities, Units and Symbols in Physical Chemistry;* 4th ed.; Royal Society of Chemistry, 2023 Abridged Version.
154. Miani, A.; Tennyson, J. Can *ortho–para* transitions for water be observed? *J. Chem. Phys.* **2004,** *120*, 2732–2739.
155. Barber, R. J.; Tennyson, J.; Harris, G. J.; Tolchenov, R. N. A high-accuracy computed water line list. *Mon. Not. R. Astron. Soc.* **2006,** *368*, 1087–1094.
156. Mondelain, D.; Mikhailenko, S. N.; Karlovets, E. V., et al. Comb-Assisted Cavity Ring down Spectroscopy of ^{17}O Enriched Water between 7443 and 7921 cm^{-1}. *J. Quant. Spectrosc. Rad. Transf.* **2017,** *203*, 206–212.
157. Vasilchenko, S.; Mikhailenko, S. N.; Campargue, A. Water Vapor Absorption in the Region of the Oxygen A-Band near 760 nm. *J. Quant. Spectrosc. Rad. Transf.* **2021,** *275*, 107847.
158. Vasilchenko, S.; Mikhailenko, S. N.; Campargue, A. Cavity Ring down Spectroscopy of Water Vapour near 750 nm: A Test of the HITRAN2020 and W2020 Line Lists. *Mol. Phys.* **2022,** *120*, e2051762.
159. Koroleva, A.; Mikhailenko, S. N.; Kassi, S., et al. Frequency Comb-Referenced Cavity Ring-down Spectroscopy of Natural Water between 8041 and 8633 cm^{-1}. *J. Quant. Spectrosc. Rad. Transf.* **2023,** *298*, 108489.
160. Conway, E. K.; Gordon, I. E.; Kyuberis, A. A., et al. Accurate Line Lists for $H_2{}^{16}O$ and $H_2{}^{18}O$ with Extensive Comparisons to Theoretical and Experimental Sources Including the HITRAN 2016 Database. *J. Quant. Spectrosc. Rad. Transf.* **2020,** *241*, 106711.
161. Conway, E. K.; Gordon, I. E.; Tennyson, J., et al. A Semi-Empirical Potential Energy Surface and Line List for $H_2{}^{16}O$ Extending into the near-Ultraviolet. *Atmos. Chem. Phys.* **2020,** *20*, 10015–10027.
162. Mikhailenko, S.N. Personal communication, 2024.
163. Coheur, P.-F.; Bernath, P. F.; Carleer, M.; Colin, R.; Polyansky, O. L.; Zobov, N. F.; Shirin, R. J. B. S. V.; Tennyson, J. A 3000 K laboratory emission spectrum of water. *J. Chem. Phys.* **2005,** *122*, 074307.

164. Mazzotti, F.; Naumenko, O. V.; Kassi, S., et al. ICLAS of Weak Transitions of Water between 11 300 and 12 850 cm^{-1}: Comparison with FTS Databases. *J. Mol. Spectrosc.* **2006,** *239*, 174–181.
165. Campargue, A.; Mikhailenko, S. N.; Lohan, B. G., et al. The Absorption Spectrum of Water Vapor in the 1.25 μm Atmospheric Window (7911–8337 cm^{-1}). *J. Quant. Spectrosc. Rad. Transf.* **2015,** *157*, 135–152.
166. Campargue, A.; Mikhailenko, S.; Liu, A. W. ICLAS of Water in the 770 nm Transparency Window (12746–13558 cm^{-1}). Comparison with Current Experimental and Calculated Databases. *J. Quant. Spectrosc. Rad. Transf.* **2008,** *109*, 2832–2845.
167. Mikhailenko, S.; Vasilchenko, S.; Campargue, A. A Recommended Line List for Water Vapor in the 12969–13418 cm^{-1} Interval. *J. Quant. Spectrosc. Rad. Transf.* **2024,** *326*, 109099.
168. Wilkinson, M. D.; Dumontier, M.; Aalbersberg, I. J., et al. *The FAIR Guiding Principles for Scientific Data Management and Stewardship*. *Sci. Data*, 3, **2016;** pp. 1−9.
169. Gordon, I. E.; Potterbusch, M. R.; Bouquin, D.; Erdmann, C. C.; Wilzewski, J. S.; Rothman, L. S. Are your spectroscopic data being used?*J. Mol. Spectrosc.* **2016,** *327*, 232–238.
170. Pickett, H. M. The fitting and prediction of vibration-rotation spectra with spin interactions. *J. Mol. Spectrosc.* **1991,** *148*, 371–377.
171. Western, C.M. PGOPHER, a program for simulating rotational structure, last accessed on February 13, 2025.
172. Chung, H.-K.; Braams, B. J.; Bartschat, K.; Császár, A. G.; Drake, G. W. F.; Kirchner, T.; Kokoouline, V.; Tennyson, J. Uncertainty estimates for theoretical atomic and molecular data. *J. Phys. D: Appl. Phys.* **2016,** *49*, 363002.
173. Lodi, L.; Tennyson, J. Line Lists for $H_2{}^{18}O$ and $H_2{}^{17}O$ Based on Empirical Line Positions and *ab Initio* Intensities. *J. Quant. Spectrosc. Rad. Transf.* **2012,** *113*, 850–858.